Competitive Reaction of Neptunium(V) and Uranium(VI) in Potassium Sodium Carbonate Rich Aqueous Media – Speciation study with focus on high resolution X-ray spectroscopy

Tonya Vitova,[1,] Ivan Pidchenko,[1] Dieter Schild,[1] Tim Prüßmann,[1] Vanessa Montoya,[1,#,] David Fellhauer,[1] Xavier Gaona,[1] Elke Bohnert,[1] Jörg Rothe, Robert J. Baker,[2*] Horst Geckeis[1]*

[1] Karlsruhe Institute of Technology, Institute for Nuclear Waste Disposal (INE), P.O. 3640, D-76021 Karlsruhe, Germany

[2] School of Chemistry, University of Dublin, Trinity College, Dublin 2, Ireland.

KEYWORDS: Neptunium, uranium, actinides, carbonate, HR-XANES, EXAFS.

ABSTRACT

Np(V) and U(VI) are precipitated from an aqueous potassium-sodium containing carbonate rich solution and the solid phases are investigated. U/Np $M_{4,5}$ edge high energy resolution X-ray absorption near edge structure (HR-XANES) spectroscopy, Np 3d4f resonant inelastic X-ray scattering (3d4f RIXS) are applied in combination with thermodynamic calculations, U/Np L_3 edge XANES and extended X-ray absorption fine structure (EXAFS) studies to analyze the local atomic coordination and oxidation states of U and Np. The XANES/HR-XANES analyses are supported by *ab-initio* quantum chemical computations with the finite difference method near edge structure code (FDMNES). The solid precipitates are also investigated with powder X-ray diffraction (pXRD), scanning electron microscopy – energy dispersive X-ray spectroscopy (SEM-EDX) and Raman spectroscopy. The results strongly suggest that $K[Np(V)O_2CO_3]_{(cr)}$, $K_3[Np(V)O_2(CO_3)_2]_{(cr)}$ and $K_3Na[U(VI)O_2(CO_3)_3]_{(cr)}$ are the predominant Np and U solid phases formed. Despite the 100 times lower initial Np(V) concentration at pH 10.5 and oxic conditions, Np(V) rich phases predominately precipitate. Prevailing formation of Np(V) over U(VI) solids demonstrate the high structural stability of Np(V) carbonates containing potassium. It is illustrated that the Np M_5 edge HR-XANES spectra are sensitive to changes of the Np-O axial bond length for neptunyl(V)/(VI).

INTRODUCTION

Neptunium-237 is an actinide with a long half-life (2.14×10^6 years) and high specific activity presenting a complex redox and coordination chemistry in aqueous systems which makes it difficult to study. For example, Np(V) carbonates have been investigated with a variety of spectroscopic techniques,[1] whereas a few examples of Np(VI) carbonates exist.[2] Only few investigations exist regarding the interaction of Np with different minerals by adsorption or structural incorporation. Balboni et al. have shown that the incorporation of Np into carbonate

minerals such as calcite ($CaCO_3$), aragonite ($CaCO_3$) and strontianite ($SrCO_3$) is possible.[3] Extended X-ray absorption fine structure (EXAFS) was applied to study the speciation of Np co-precipitated with calcite[4] and sorbed[5] onto calcite. Studies dedicated to the interaction of Np with other minerals are even more scarce and focus mainly on Fe(II) bearing minerals. When Np(V) reacts with certain iron(II) phases, depending upon the conditions, reduction to Np(IV)[6] and either sorption or precipitation has been observed.[7]

Depending on the geochemical conditions of the environment, different U alteration products are expected.[8] For example, within the weathered U ore minerals, the mixed U(VI)/(V) oxidation state mineral wyartite ($CaU(V)[(UO_2)_2(CO_3)O_4(OH)]\cdot 7H_2O$) can be formed after oxidation of uraninite (UO_2). This mineral can potentially incorporate minor pentavalent actinides (An) like neptunium (Np(V)) and plutonium (Pu(V)).[9] On the other hand, different U minerals were used in the literature to study the reactivity of Np with them, observing that ^{237}Np was sorbed onto their surface or pure Np solid phases were formed. It was also found that Np can be incorporated into the mineral structure by cation exchange or by substitution of a U(VI) for a Np(V) or (VI) ion in the mineral framework, with or without a compensating charge balancing cation substitution.[10] Within the available experimental data, it seems that the structure and/or chemical composition of the U mineral phase is of direct importance to the amount of incorporated Np.[11] In this sense, several laboratory studies have already illustrated that the U alteration products can effectively retain Np by sorption of incorporation processes but then subsequently release it into the aqueous solution.[10]

In this work, we investigate the reactivity of U(VI) and Np(V) in a competitive reaction with high content of carbonate and the presence of potassium and sodium in the aqueous solution. The focus of our study is on the speciation of the products formed by co-precipitation reactions of Np(V)

during the syntheses of the U(VI) carbonate phase grimselite ($K_3Na[UO_2(CO_3)_3]\cdot H_2O_{(cr)}$). We apply the Np 3d4f resonant inelastic X-ray scattering (3d4f RIXS) and Np M_5 edge high-energy resolution X-ray absorption near edge structure (HR-XANES) experimental techniques. These are used here for the first time for determination of the oxidation state of Np.[12] Their sensitivity to the U/Np=O axial bond length in actinyls is also discussed. The An $M_{4,5}$ edge HR-XANES gives a significant advantage[12a] over the widely applied conventional An L_3 edge XANES mode in studies related to the oxidation states and the electronic structure of the An elements.[13] It is very sensitive to minor amounts of An oxidation states in mixtures and directly probes the An 5f unoccupied states, which are sensitive to changes in the chemical bonding. In addition to Np M_5 and U M_4 edge HR-XANES/3d4f RIXS, we also applied powder X-ray diffraction (pXRD), scanning electron microscopy energy dispersive X-ray spectroscopy (SEM-EDX), Raman spectroscopy and U/Np L_3 edge XANES and EXAFS techniques as well as thermodynamic calculations. Computations of U/Np L_3, Np M_5 and U M_4 and M_5 edge HR-XANES spectra are performed with the *ab-initio* finite difference method near edge structure (FDMNES) code based on the multiple scattering theory.[23b] The combination of conventional and modern spectroscopic tools and thermodynamic calculations gives conclusive evidence for the Np and U oxidation states and coordination environment and thereby provide knowledge about the chemical behavior of Np(V) when precipitated with higher amounts of U(VI) in a K-Na-CO_3-H_2O system.

MATERIAL AND METHODS

Caution! ^{237}Np is a radioactive isotope and an α-emitter. It should be handled in dedicated facilities with appropriate equipment for radioactive materials to avoid health risks caused by radiation exposure.

Synthesis. A **grimselite** ($K_3Na[UO_2(CO_3)_3]\cdot H_2O_{(cr)}$) reference sample was synthesized according to the procedure reported in the literature.[14] A Np stock solution was prepared from 16.2 mg of $^{237}Np(V)$ aqua complex dissolved in 0.055 M $HClO_4$ to give a total volume of 9.86 mL. The [Np] = 6.9×10^{-3} M concentration was determined by liquid scintillation counting. Under ambient conditions, a vial was charged with $UO_2(NO_3)_2\cdot6H_2O$ ([U] = 9.9×10^{-3} M, [NO_3] = 1.8×10^{-2} M), Na_2CO_3 ([Na] = 0.24 M), K_2CO_3 ([K] = 0.74 M), $[CO_3]_{TOT}$ = 0.49 M solutions and MQ-water with 20 mL total volume. 0.246 mL of Np(V) stock solution was then added and the vial stoppered. The resulting [U] and [Np] in the aqueous solution were 9.9×10^{-3} M and 8.4×10^{-5} M, respectively. The pH was about 10.5 and the conditions were oxic. After standing for 2 weeks, a light-green precipitate formed, which was isolated, quickly washed with water (2 × 1 mL) and samples were prepared for the measurements. The following nomenclature is used: **Np-cp** - Np in Np(U) precipitate, **U-cp** - U in Np(U) precipitate, **grimselite** ($K_3Na[UO_2(CO_3)_3]_{(cr)}$) and **metaschoepite** ($UO_3\cdot nH_2O$, n < 2) used as a reference and prepared via the literature procedure and confirmed by pXRD and vibrational spectroscopy.[15]

pXRD, SEM-EDX and Raman spectroscopy. pXRD patterns for both **grimselite** and the Np(U) precipitate were collected using a Bruker AXS D8 powder diffractometer equipped with a BSI (Baltic Scientific Instrument) Si(Li) solid detector and a Cu K_α X-ray source. The Np(U) precipitate was studied by SEM-EDX applying a commercial Quanta 650 FEG (FEI, The Netherlands) equipped with a silicon drift X-ray detector (Thermo Scientific, model UltraDry). The Raman spectra were measured at room temperature using a Bruker Sentera dispersive Raman microscope at 532 nm excitation wavelength; a few small crystals of the Np(U) precipitate were placed into a 1 mL glass vial and dried onto inner wall surface.

X-ray Absorption Spectroscopy (XAS). The U/Np L_3 edge EXAFS and Np/U $M_{4,5}$ edges HR-XANES/3d4f RIXS measurements were performed at the INE-Beamline, Karlsruhe Research Accelerator (KARA), Karlsruhe, Germany.[16] Two Ge(422) and two Si(111) crystals were mounted in the double crystal monochromator (DCM) for An L_3 or $M_{4,5}$ edge XAS measurements, respectively. The beam was focused to ~0.5 mm vertically and ~0.5 mm horizontally onto the sample. For the U/Np $M_{4,5}$ edge HR-XANES experiments, the Np(U) precipitate was placed into a double containment aluminum cell, where the inner compartment was sealed by 8 µm and the outer compartment by 13 µm Kapton foil, respectively (Figure S1). The **grimselite** and **metashoepite** references were mixed with cellulose and pressed as pellets. Np M_5 and U M_4 edges XANES spectra were measured in high-energy resolution mode (HR-XANES) using an X-ray emission multi analyzer crystal spectrometer (MAC-Spectrometer).[17,18] The MAC-Spectrometer was also applied for Np 3d4f RIXS measurements. The sample, five Si(220) analyzer crystals and a detector (single diode silicon drift detector, SDD Vortex) were positioned on a Rowland circle in the vertical plane with diameter of 1 m equal to the bending radius of the spherically bent analyzer crystals. The MAC-Spectrometer was set at the maximum of the Np M_α (M_5N_7, E = 3261 eV) and U M_β (M_4N_6, E = 3337.0 eV) emission lines at 81.92° and 75.36° Bragg angles, respectively. The energies of the emission lines and the absorption edges are taken from the program PyMca[19] since the energies of the M_5N_7 and M_5N_6 emission lines are listed separately, in contrast to the program Hephaestus[20] previously used. A glovebox filled with He and equipped with a lock chamber for transfer of samples was built around the MAC-Spectrometer to minimize loss of X-ray intensity during the measurements in the tender X-ray range - Np M_5 (E = 3664 eV) and U M_4 (E = 3726 eV) absorption edges. A constant He flow was maintained; the O_2 level was monitored continuously and kept constant (~ 0.1%) inside the glovebox. The experimental energy

resolution during the Np M_5 edge HR-XANES measurements was 1.0 eV, which was determined by measuring the full width at half maximum (FWHM) of the elastic peak at 81.92° Bragg angle of the analyzer crystals. The DCM was calibrated setting the energy position of the main absorption maximum (white line, WL) of the U M_4 edge HR-XANES spectrum of a reference UO_2 sample to 3725.2 eV. Np/U M_5/M_4 edge HR-XANES and normal emission spectra of $NpO_{2(am,hyd)}/UO_2$ were measured after each sample to verify the energy calibration of the DCM and the alignment of the MAC-Spectrometer. No shifts of the normal emission lines measured for each sample were found during the experiments. For recording the Np 3d4f RIXS maps and the HR – XANES spectra the following parameters were applied: Np RIXS – excitation energy 3659 – 3684 eV, 0.5 eV step size, emission energy 3248 – 3268 eV, 0.25 eV step size, 2 s integration time; U M_4 and Np M_5 edge HR-XANES – the energy ranges are relative to the main absorption maximum: -15 - -5 eV, 0.5 eV step size, -5 - +15, 0.1 eV step size, +15 – +65, 0.5 eV step size, 1 s integration time. The INE-Beamline is a bending magnet beamline with < 10^9 ph/s onto the sample at 3-4 keV. We first measured Np(VI) in aqueous solution, which is much more sensitive to radiation damage; we did not observe any damage for this liquid material. We measured several spectra for each of the Np and U solid samples and did not observe any changes.

For the U and Np L_3 edge EXAFS measurements of the Np(U) precipitate, a sample aliquot was placed into 300 µl Eppendorf vials in air. The oscillating $\chi(k)$ (EXAFS) part of the X-ray absorption fine structure (XAFS) spectrum was extracted, Fourier transformed (FT) and modelled by using the ATHENA and ARTEMIS programs, respectively, parts of the IFFEFIT program package.[20] The $\chi(k)$ spectra within 2.6-10.4 $Å^{-1}$ range for **Np-cp**, 2.6-8.6 $Å^{-1}$ for **U-cp** and 2.6-10.6 $Å^{-1}$ for **grimselite** were weighted by k = 1, 2 or 3 and Hanning windows with sills equal to 2 (dk=2) were applied. The fits were performed in R space for 1.0-3.0 Å range (**Np-cp)** and for 1.0-4.1 Å

(**U-cp** and **grimselite)**. Three shells were modeled for Np: two Np-O and one Np-C distances and four shells for U: two U-O, one U-C and one U-K distances. Structures of $K_3[NpO_2(CO_3)_2]\cdot nH_2O_{(cr)}$ (reproduced from Volkov et al.[21]) and grimselite mineral $K_3Na[(UO_2)(CO_3)_3]\cdot H_2O_{(cr)}$ (AMCSD 0005731) were used as initial models for the fit of the Np and U EXAFS spectra, respectively. The FEFF input files were generated by the FEFF9.6 *ab-initio* quantum chemical theoretical code based on the multiple scattering theory.[22] The scattering potentials were calculated for a cluster of 59 atoms by including the self-consistent field loop (SCF 4.0). The amplitude reduction factor (S_0^2) was set to 0.8 for Np and U, which is an average value as determined for previous EXAFS measurements performed in florescence mode at the INE-Beamline. The shells of the Np FT-EXAFS spectrum were fit in the following order: Np-O1, Np-O2, Np-C and for U FT-EXAFS in the order: U-O1, U-O2, U-C and U-K. For each shell, initially the interatomic distances (R) were varied, while the coordination numbers (N) were fixed; N and R were consecutively varied until the best fit was obtained; this procedure was repeated for each shell. The Debye-Waller factors (DW) and the energy shifts of the ionization potential (ΔE_0) were always varied. The number of variables was kept approximately half the number of independent data points during the fitting procedure. A goodness of fit parameter (r) within 0.004-0.007, which is 0.4-0.7% difference between data and model, was obtained for the fits. The ΔE_0 parameters were found around 7.4(1) for **Np-cp**, 4.3(4) for **U-cp** and 3.2(8) for **grimselite** (for details see Table 1).

Computations of U and Np L_3 edge XANES and $M_{4,5}$ edge HR-XANES spectra. U and Np L_3 edge XANES and the $M_{4,5}$ edge HR-XANES as well as DOS spectra were computed with the FDMNES code.[23] These *ab-initio* calculations were performed for a cluster with 6 Å radius (≈ 60 atoms, L_3 edge)/3.5 Å radius ($M_{4,5}$ edge) using Green's function formalism, muffin-tin potentials (L_3) or finite difference method ($M_{4,5}$) and taking into account spin-orbit interactions. The Fermi

energy was determined using self-consistent field (SCF) calculations. The calculation approach described in T. Vitova at al.[12f] was used for the calculations of the $M_{4,5}$ edge spectra. The calculated U M_4 and Np M_5 edge HR-XANES spectra with and without quadrupole transitions are identical. The calculated L_3 spectra were convoluted using the default values of FDMNES and experimental broadening was not included. The convolution parameters for the $M_{4,5}$ HR-XANES spectra are given in SI. Example of input files are provided in SI too. The U L_3 edge spectra were calculated for the following crystal structures: $K_3Na[UO_2(CO_3)_3]\cdot H_2O_{(cr)}$ (grimselite – ICSD 186867; Figure S4 depicts the **grimselite** spectrum calculated using AMCSD 0005731, which is very similar), $UO_2CO_3\cdot H_2O$ (rutherfordine - ICSD 87760) and Np L_3 edge spectra for $K[NpO_2CO_3]_{(cr)}$ (ICSD 15685, Pu is exchanged with Np, lattice parameters: a = b = 5.09, c = 9.83 Å) and $K_3[NpO_2(CO_3)_2]_{(cr)}$ (reproduced from Volkov et al.[21]) were calculated. We verified this approach by applying the same crystal structure - **grimselite** with either U or Np and found that the spectra are very similar as it can be expected for Z ± 1 difference (Figure S5). For the calculation of the Np L_3 edge XANES of $K[NpO_2CO_3]_{(cr)}$ the lattice parameters: a = b = 5.12, c = 9.971 Å reported by Keenan and Kruse[24] were also applied; the spectrum is similar to the spectrum calculated for ICSD 15685 and exchanging Pu with Np (Figure S6). We verified the influence of the cluster size on the spectra by increasing the size of the atomic cluster to 7 Å for grimselite (94 atoms) and rutherfordine (100 atoms). The computed spectra do not considerably differ (not shown). U M_4 and M_5 edge HR-XANES and DOS spectra were calculated for **grimselite**. Np M_5 edge HR-XANES and DOS were calculated for $K[NpO_2CO_3]_{(cr)}$ and $K_3[NpO_2(CO_3)_2]_{(cr)}$. In both cases the same structures as for the L_3 edge calculations were used.

Thermodynamic Calculations. Calculations were performed at 25 °C with the PHREEQC 3.3 code.[25] The activity coefficient formalism of SIT (Specific Interaction Theory) was used to

describe the deviations from ideal chemical behavior that occur in concentrated electrolyte media. The ThermoChimie v9.b database was selected as the primary database because it provides an internally-consistent database with SIT interaction coefficients capable of reproducing measured and observed behaviors of the Np and U systems.[26] Additionally, thermodynamic data for the potassium Np(V) carbonate solids, **grimselite** ($K_3Na[(UO_2)(CO_3)_3]\cdot H_2O_{(cr)}$) and SIT coefficients for anions with K^+ was included from Guillaumont et al.[27] However, considering the uncertainties in the thermodynamic data selection of **grimselite**, the solubility constant of this solid must be considered as only being provisional in thermodynamic calculations.

RESULTS

The synthesis of **grimselite** ($K_3Na[UO_2(CO_3)_3]\cdot H_2O_{(cr)}$) with addition of Np(V) in the solution ([Np] = 8.4×10^{-5} M and [U] = 9.9×10^{-3} M) results in an intense green precipitate. In contrast, yellow crystals of **grimselite** are obtained in the absence of Np.[14] A significantly higher Np content compared to U in this precipitate was observed from SEM-EDX ([U] below the limit of detection - cf. SEM-EDX results) and corroborated by Raman and X-ray spectroscopies (*vide infra*). The intensity of the characteristic U M_β fluorescence line is 4% of the Np M_α line (similar probability for emission) for the Np(U) precipitate suggesting that the U concentration is about 4% of the Np concentration in the sample. This strong evidence for preferential Np phase precipitation over a U phase may be explained simply by differing solubility of Np(V)[28] and U(VI) carbonates for the given experimental conditions ([K] = 0.74 M, $[CO_3]_{TOT}$ = 0.49 M, pH ~ 10.5, oxic conditions). Additionally, it is well known that potassium solid phases of Np(V) can precipitate in alkaline solutions containing large sodium and potassium concentrations, even if the concentration of Na^+ is much higher than that of K^+, which is supported by the difference of almost four orders of magnitude of the solubility constants of the solids containing potassium compared to their sodium

homologous (Equations 1-4).[29,30] The preferential precipitation could also be related to formation of a metastable solid phase of Np as described in the literature.[31] The green precipitate was analyzed by multiple techniques to identify its composition, U and Np local coordination environments and oxidation states.

$$K[NpO_2(CO_3)](s) \rightleftharpoons K^+ + NpO_2^+ + CO_3^{2-} \qquad \text{Log } K_s = -13.6 \quad (1)$$

$$K_3[NpO_2(CO_3)_2](s) \rightleftharpoons 3K^+ + NpO_2^+ + 2CO_3^{2-} \qquad \text{Log } K_s = -15.9 \quad (2)$$

$$Na[NpO_2(CO_3)](s) \rightleftharpoons Na^+ + NpO_2^+ + CO_3^{2-} \qquad \text{Log } K_s = -10 \quad (3)$$

$$Na_3[NpO_2(CO_3)_2](s) \rightleftharpoons 3Na^+ + NpO_2^+ + 2CO_3^{2-} \qquad \text{Log } K_s = -12 \quad (4)$$

SEM-EDX. Traces of crystalline K_2CO_3 phase are identified by SEM-EDX formed on K-Np(V)-CO_3 phase (Figures 1b and S2a-d). With SEM-EDX it is difficult to detect characteristic X-ray lines of U at low concentration besides intense Np lines due to their strong overlap. This is also valid for a small amount of Na in a sample with a high K content. The U concentration is estimated less than 10% of the Np concentration. Similarly the Na concentration is estimated less than 10% of the K concertation in the Np(U) precipitate. At high magnification (100kx), a granular structure is observed by SEM suggesting a particle size of roughly 50 nm. Since the volume of the characteristic X-rays generated at 30kV of the primary electron beam is much larger than 50 nm, individual particle compositions of the Np(U) precipitate cannot be distinguished by SEM-EDX.

pXRD and Thermodynamic calculations. The pXRD pattern of the Np(U) precipitate has main diffraction peaks similar to those found for $K[NpO_2CO_3]_{(cr)}$ reported by Keenan et al. and Visyashcheva et al. (Figure 1a).[32] However, the presence of $K_3[NpO_2(CO_3)_2]_{(cr)}$ cannot be excluded. $K[NpO_2CO_3]_{(cr)}$ is reported to form by adding K_2CO_3 to Np(V) (10^{-5}–10^{-7} M) dilute acid solutions obtaining final carbonate concertation < 0.2 M, whereas $K_3[NpO_2(CO_3)_2]_{(cr)}$ is preferably

formed in more concentrated K_2CO_3 solutions (~0.5-2.0 M).[32,33] For 0.2-0.5 M K_2CO_3 solutions (this study) a metastable K-Np(V)-CO_3 system is formed where depending on conditions either $K[NpO_2CO_3]_{(cr)}$ or $K_3[NpO_2(CO_3)_2]_{(cr)}$ phase precipitates or even coexist.[33] According to thermodynamic calculations, $K_3[NpO_2(CO_3)_2]_{(cr)}$ is predicted to be formed under the conditions selected for the present study (Pourbaix diagram in Figure 2b); however, it should be kept in mind that large uncertainties are expected in these simulations due to the combination of high ionic strength of the system (i.e. ~1 M), presence of highly charged species in the aqueous solution (i.e. $NpO_2(CO_3)_3^{5-}$) and some unknown SIT coefficients in the thermodynamic database. The $K[NpO_2CO_3]_{(cr)}$ and $K_3[NpO_2(CO_3)_2]_{(cr)}$ phases have distinct structural differences but a similar design of the anionic layers $[NpO_2(CO_3)_x]^{(-2x+1)}$ (x = 1 or 2) (Figure 3); in both compounds the NpO_2^+ ion is coordinated by six oxygen atoms originating from three carbonate ligands in the equatorial plane. The $K[NpO_2CO_3]_{(cr)}$ phase forms a hexagonal structure consisting of $[NpO_2CO_3]^-$ anionic layers with K^+ ions located in between the layers. The $K_3[NpO_2(CO_3)_2]_{(cr)}$ phase has an orthorhombic structure where half of the NpO_2^+ moieties are replaced by K^+ ions. The $[NpO_2(CO_3)_2]^{3-}$ anionic layers are located at 1/2·*c* crystallographic intervals and polymerize such that {–K–O=Np=O–K–O=Np=O–K–} infinite chains are formed along the *c* axis with closest Np-K atoms being found in the adjacent anionic layers.[21] Depending on the structure of the K-NpO_2-CO_3 phase, 0.5 to 2.0 H_2O were reported to enter the structure, which are randomly distributed about the fourfold positions between the anionic layers, and likely enhancing the stability of the compound.[21] In the $M[NpO_2CO_3]_{(cr)}$ structures (M = Li, Na, K) bond distance parameters vary depending on the alkaline metal, which define the structural variations with an orthorhombic to hexagonal transformation on the Na-K boundary.[33b]

In Figure 1a, the most intense and narrow pXRD peak detected at $2\theta \approx 29°$ (highlighted with a black arrow) can be assigned to one of the uranyl carbonate phases, either **rutherfordine** ($[UO_2CO_3]\cdot H_2O_{(cr)}$) or **grimselite** ($K_3Na[(UO_2)(CO_3)_3]\cdot H_2O_{(cr)}$). The latter option is supported by the thermodynamic calculations, albeit with considerable uncertainties in the simulation, and the same caveats as in the case of Np also apply (Pourbaix diagram in Figure 2a). The structure of **grimselite** is different to the potassium neptunyl carbonates described above as it consists of a typical uranyl tricarbonate cluster $[(UO_2)(CO_3)_3]^{3-}$ forming a hexagonal bipyramid interconnected through bonds to Na and K polyhedra via $U{=}O\cdots M^+$ interactions,[14] whilst the structure of rutherfordine contain sheets of uranyl carbonate polyhedra (Figure 3).[34]

Raman spectroscopy. Raman spectroscopy reveals bands for the Np(U) precipitate associated with the symmetric –yl stretching: $\nu_1(Np{=}O) = 768\ cm^{-1}$; $\nu_1(U{=}O) = 821\ cm^{-1}$ (Figure 1c). The Np=O stretch can be compared to that of $Na_3[NpO_2(CO_3)_2].nH_2O_{(cr)}$ ($\nu_1(Np{=}O) = 772\ cm^{-1}$),[1d] as the spectrum for $M[NpO_2CO_3]_{(cr)}$ is not reported in the literature, whilst the uranyl stretch is similar to that in grimselite ($\nu_1(U{=}O) = 815\ cm^{-1}$)[35] or in $UO_2CO_3\cdot H_2O_{(cr)}$ ($\nu_1(U{=}O) = 837\ cm^{-1}$).[36] The Raman spectra also exhibit bands typical for the asymmetric deformation - ν_4 of the carbonate ion at 716 cm^{-1} and three bands at 1060, 1070 and 1086 cm^{-1} corresponding to ν_1 symmetric stretch.

U and Np L_3 edge EXAFS. To gain further insights into the local atomic environments of Np and U, we conducted an L_3 edge EXAFS spectroscopic study of Np and U in the Np(U) precipitate (**Np-cp** and **U-cp**). **Grimselite** ($K_3Na[(UO_2)(CO_3)_3]\cdot H_2O_{(cr)}$) was also investigated as a suitable U reference. The Np and U L_3 edge FT-EXAFS spectra and their best fits are depicted in Figure 4a-c. The Np FT-EXAFS spectrum of the **Np-cp** reveals two intense peaks originating from scattering of the photoelectron from axial and equatorial O ligands (Figure 4a). The analyses result in two axial O atoms at an average distance (R) R(Np-O)ax = 1.83(1) Å from Np and in six equatorial O

atoms at R(Np-O)eq = 2.53(1) Å originating from three carbonates with R(Np-C) = 2.99(4) Å (Table 1). The EXAFS fits performed using three shells (O1 + O2 + C) or two shells (O1 + O2) showed that the data is better described with a three-shell model (see Figure S3, Table S1). The structure obtained from pXRD for $K_3[NpO_2(CO_3)_2]\cdot nH_2O_{(cr)}$ exhibits the following average values for R(Np-O)ax = 1.80 Å, R(Np-O)eq = 2.58 (R(Np-C) is not reported).[21] The coordination of Np in $K[NpO_2CO_3]_{(cr)}$ has a more significant discrepancy for the axial bond R(Np-O)ax = 1.96 Å, whereas the average equatorial R(Np-O)eq = 2.57 Å bond and R(Np-C) = 2.96 Å are similar (cf. Table 1 and 2). No clear contribution from K atoms can be found in the EXAFS spectrum; K atoms are expected at ~3.8 Å (6 atoms) for $K[NpO_2CO_3]_{(cr)}$.

In Table 1 the EXAFS best-fit structural parameters for **grimselite** ($K_3Na[(UO_2)(CO_3)_3]\cdot H_2O_{(cr)}$) are listed - (R(U-O)ax = 1.80(1) Å, R(U-O)eq = 2.41(1) Å, R(U-C) = 2.90(1) Å) and are close to those determined by X-ray crystallography for **grimselite** (R(U-O)ax = 1.78 Å, R(U-O)eq = 2.42 Å, R(U-C) = 2.89 Å).[14] The 0.08 Å elongation of the R(U-K) found from the EXAFS fit (EXAFS: R(U-K) = 3.98(3) Å, pXRD: R(U-K) = 3.89 Å) might indicate structural disorder as EXAFS measures an average of the local coordination environments of all U atom, whereas pXRD is sensitive only to the long-range atomic order in the material.

The structural parameters for **U-cp** slightly differ compared to **grimselite** ($K_3Na[(UO_2)(CO_3)_3]\cdot H_2O_{(cr)}$); there is 0.02(1) and 0.03(1) Å shortening and elongation of the axial and equatorial U-O bonds, respectively (R(U-O)ax = 1.78(1) Å, R(U-O)eq = 2.44(1) Å) (Table 1 and 2). This result agrees with the Raman spectroscopy and the U M_4 edge HR-XANES results (*vide infra*). Comparable U-C coordination numbers (N) and interatomic distances for **U-cp** (N = 3.1(8), R(U-C) = 2.91(2) Å) and **grimselite** (N = 2.8(6), R(U-C) = 2.90(2) Å) are found (Table 1) suggesting formation of similar uranyl tricarbonate compounds. The interatomic distances for

rutherfordine ($UO_2CO_3 \cdot H_2O_{(cr)}$, ICSD 87760) deviate more substantially: R(U-O)ax = 1.74 Å, R(U-O)eq = 2.44-2.52 Å, R(U-C) = 2.94 Å.

Both actinide elements are coordinated by carbonate but interestingly the peak corresponding to K cannot be identified clearly in the Np L_3 edge FT-EXAFS, whereas it is well visible in both U L_3 edge FT-EXAFS spectra, presumably due to the poor crystallinity of the Np solid phases (cf. Figure 4b,c).

No indication for coordination of U/Np with Np/U is found in the three FT-EXAFS spectra due to very long R(U/Np-Np/U) distance and/or disorder effects, e.g. R(U-U) ~ 6.77 Å for **grimselite** ($K_3Na[(UO_2)(CO_3)_3] \cdot H_2O_{(cr)}$). Also, it must be remembered that EXAFS is usually not sensitive to Z differences of ± 1.

U and Np L_3 edge XANES. We compared experimental and calculated with the FDMNES code U and Np L_3 edge XANES spectra. Those spectra fingerprint the local atomic environment of all U or Np atoms in the materials therefore the analyses are complementary to XRD and EXAFS. The U L_3 edge XANES experimental spectra for **U-cp** and **grimselite** (Figure 5) are almost identical and very similar to the U L_3 edge calculated spectra of grimselite ($K_3Na[(UO_2)(CO_3)_3] \cdot H_2O_{(cr)}$) and rutherfordine ($UO_2CO_3 \cdot H_2O_{(cr)}$). The energy positions of peaks C and D in the experimental Np L_3 edge XANES spectrum of **Np-cp** are shifted to lower energies compared to the spectra of **U-cp** and **U-pg**. Thus the **Np-cp** spectrum is more similar to the computed spectra of $K[NpO_2CO_3]_{(cr)}$ and $K_3[NpO_2(CO_3)_2] \cdot nH_2O_{(cr)}$, in agreement with EXAFS and XRD results. Note that the spectra are plotted on a relative energy scale and we did not find significant differences by calculating U or Np L_3 edge XANES for the same crystal structure (Figure S4). The main absorption peaks (white line, WL) for the calculated spectra has much higher intensity since no experimental broadening is taken into account in the computations. The

energy positions of the WLs of the U and the Np L_3 edge XANES spectra correspond to oxidation states U(VI) and Np(V). The spectra are compared to reference compounds in Figures S7 and S8.

Np 3d4f RIXS. To obtain further information on the oxidation state and coordination environment, we applied U M_4 edge HR-XANES and Np 3d4f RIXS and M_5 edge HR-XANES spectroscopy.[12] Spectra for reference compounds containing Np in its +IV, +V and +VI oxidation states were also recorded, namely $Np(IV)O_{2(am,hyd)}$, $Ca_{0.5}Np(V)O_2(OH)_2 \cdot 1.3H_2O_{(cr)}$ and $Na_2Np(VI)_2O_{7(cr)}$ (Figures 6 and 7).[37,38]

The Np 3d4f RIXS map is a two dimensional representation of the Np M_α emission line measured across the Np M_5 absorption edge.[12f] The Np M_5 edge HR-XANES spectrum is a cross section of the RIXS map at a constant emission energy, i.e. the emission intensity integrated within 0.1 eV emission energy range is plotted as a function of the excitation energy. Usually the HR-XANES is extracted at the maximum of the normal emission line measured at excitation energy well above the main absorption peak (green line in Figure 6). However, we recently showed for U, Np and Pu that the main resonant peak (the most intense structure in the RIXS maps) can be shifted to higher emission energies with respect to the normal emission line depending on the material (shift between red and green lines in the RIXS maps in Figure 6). This shift was explained with variations of the interaction of the 3d excited electron in the 5f states and the created 4f core-hole and was correlated to the level of localization of the 5f states.[12f] If the excited electron is in a more localized 5f states, the interaction will be stronger and the energy shift between normal and resonant emission will be larger. The energy shifts between normal and resonant emission for the Np(IV), Np(V) and Np(VI) reference compounds – 1.0 ± 0.1 eV (Np(IV) and Np(V)) and 0.5 ± 0.1 eV (Np(VI)) (Figure 6 a-c). According, the 5f states are more delocalized for the Np(VI) compound and similarly localized for the Np(IV) and Np(V) compounds. This energy shift is 0.7 ± 0.1 eV for

the Np 3d4f RIXS of the Np(U) precipitate (Figure 6 d). Note that the oxidation state, but also coordination environment and crystal structure can influence the level of localization of the 5f states and thereby the magnitude of this energy shift. Since our references are oxides whereas the Np(U) solid is a carbonate material a specific trend might not be observed, nevertheless the energy shift for Np(U) is in between the values found for Np(V) and Np(VI). We recently observed that this energy shift in the An 3d4f RIXS maps also depends on the experimental energy resolution (not shown), therefore RIXS maps should be measured at the same experimental conditions to allow for any comparison. We plotted the cross section of the main resonant peak along the emission and excitation energy axis (violet lines in Figure 6). It is clearly visible that the energy positions of the maxima of these cross sections, the resonant emission (red line on the right of the RIXS maps) and the main peak of the HR-XANES extracted at the maximum of the resonant peak agree well (red line on the top of the RIXS maps). In contrast, the HR-XANES extracted at the normal emission maxima and the normal emission lines are shifted to lower energy (green lines in Figure 6). The main absorption peak of these HR-XANES spectra is a cross section of the tail of the broadening of the resonant peak therefore it does not measure the absorption cross section and might be not appropriate for any quantitate analyses like oxidation states analyses applying a linear combination least squares fit. We also simulated the conventional Np M_5 edge XANES spectra by integrating a larger (17 eV) emission energy region across the RIXS maps (magenta rectangle in Figure 6). It is clear that this Np M_5 edge XANES spectra (magenta line on the top of the RIXS maps) has one broad peak and does not show any fine structure as the HR-XANES spectra (green and red lines on the top of the RIXS maps). Due to the asymmetric distribution of intensity with respect to the maxima of the normal emission lines (green lines), the conventional XANES spectra are shifted to higher energy compared to the HR-XANES spectra (top of RIXS maps). Further

details on the contributions of core-hole lifetime and experimental broadening to the RIXS maps are given in Vitova et al.[12f]

U and Np $M_{4,5}$ edge HR-XANES The Np M_5 edge HR-XANES spectra of the Np(U) precipitate (**Np-cp** and **U-cp**) and the Np(IV), Np(V) and Np(VI) reference compounds are depicted in Figures 7a and 8a. The Np(V) and Np(VI) compounds generally contain an axial Np trans-dioxo moiety (O=Np=O) with a typical short bond length of less than about 1.80 Å (neptunyl). The elongated bond is referred to as neptunate. The energy position of the main absorption peak (A) of the Np M_5 edge HR-XANES spectra shifts + 0.3 ± 0.05 eV from Np(IV) to Np(V) and + 0.6 eV ± 0.05 eV from Np(V) to Np(VI) (Table 3). The small + 0.3 ± 0.05 eV energy shift between Np(IV) and Np(V) is not unusual since Np(V)-yl forms a covalent bond with the 2 axial O atom and as a result there is shift of electronic density towards Np(V) leading to energy shift of the absorption edge of the spectrum to lower energies. For example for Np L_3 edge XANES, the order is revers – the spectrum of Np(V)-yl is at lower energies compared to Np(IV).[39]

The oxidation state of Np in Np(U) does not change from the initial +5 as evidenced by the position of peak A at 3667.9 eV, which is only 0.1 eV lower than that for the Np(V) reference spectrum. Similar minor energy shifts of the main peak are found for U M_4 edge HR-XANES spectra for a series of U(VI) materials and are explained by different electronic density on the U(VI) atom depending on its short and long range atomic environments.[40]

Peak C located at higher energies is well resolved in the Np M_5 edge HR-XANES spectra of the Np(VI), Np(V) references and the Np(U) solid. Peak B, present in the U M_4 edge HR-XANES spectra of uranyl(VI) (Figure 7b), is visible only in the spectrum of Np(VI) (Figure 7a) and overlaps with the main peak in the Np(V) spectra. We attribute peaks B and C to electronic transitions to π^* and σ^* molecular orbitals with predominant contributions of Np 5f and O 2p

atomic orbitals in analogy to those for U(VI)-yl resolved in U M_4 edge HR-XANES spectra.[12e] Peak A describes transitions to the δ and φ largely nonbonding U 5f orbitals (cf. simplified molecular orbital scheme for neptunyl in Figure 9). The molecular orbital schemes of uranyl and neptunyl in the ground state calculated with DFT taking into account also spin-orbit coupling are discussed in T. Vitova at al.[12e] We recently also compared ground state FDMNES calculations with multiplet calculations of Pu M_5 edge HR-XANES spectra of Pu(VI) in aqueous solution (plutonyl) and found that the computed spectra are very similar. The multiplet effects lead to broadening of the peaks but the σ* peak is well separated from the main absorption peak.[12f]

In order to compare the HR-XANES spectra measured at the U M_4 and Np M_5 absorption edges and to verify that the assignment of spectral peaks to electronic transitions to specific molecular orbitals of neptunyl is correct, we performed quantum chemical calculations of U $M_{4,5}$ and Np M_5 edge HR-XANES and f-DOS spectra with the FDMNES code (Figures 10, 11 and 12). The computed U M_4 and M_5 edge HR-XANES and the f-DOS spectra of **grimselite** are depicted in Figure 10. Due to selection rules ($\Delta J = 0, \pm 1$), $3d_{3/2} \rightarrow 5f_{5/2}$ (M_4 edge) and $3d_{5/2} \rightarrow 5f_{5/2}$, $3d_{5/2} \rightarrow 5f_{7/2}$ (M_5 edge) electronic transitions take place at the two absorption edges. In addition, the screening of the core-hole differs (multiplet effects), which also has influence on the spectra. The main differences between the U M_4 and M_5 edge HR-XANES calculated spectra depicted in Figure 10 are the overlap of the first two peaks and the higher intensity of the second peak (transitions to π*) in the M_4 HR-XANES spectrum (Figure 10 a). The well separated peak C, describing transitions to the σ* orbital, is at the same energy position in both spectra. The post-edge regions of the two spectra are identical (cf. Figure S9). Considering these results, we conclude that the assignment of the spectral peaks for Np M_5 edge HR-XANES spectrum of neptunyl is appropriate.

The computed Np M_5 edge HR-XANES and f-DOS spectra of the two Np(V) compounds - $K[NpO_2CO_3]_{(cr)}$ and $K_3[NpO_2(CO_3)_2]\cdot nH_2O_{(cr)}$ are shown in Figures 11 a and b. Similarly to the uranyl case, there is a peak in the Np f-DOS and the HR-XANES spectra corresponding to the σ* orbital (Np(VI) – at 5 eV, U(V) – at 3 eV). The U M_4 edge and the Np M_5 edge computed spectra are compared to the experimental spectra in Figure 12. The calculated and experimental spectra of **grimselite** and **U-cp** are in agreement (cf. Fgiure 12a and S10). The Np(U) sample is a mixture of the two Np(V) compounds, which is also suggested by the energy position of peak C of the experimental **Np-cp** spectrum located between the C peaks of the computed spectra of the two Np(V) reference compounds. Note that the main absorption maxima of the calculated and the experimental spectra are aligned.

The position of peak C varies significantly in all spectra (Table 3). In the previous studies it was shown that the energy shift between peaks A and C (ΔE_{C-A}) in U(VI)-yl M_4 edge HR-XANES spectra increases by shortening of the axial U-O bond length (Table 2, Figure 7b).[40],[41],[42] DFT + U calculations of the *f*-DOS of uranyl(VI) suggest that changes of equatorial U-O bond length does not influence directly $\Delta E_{C-A.}$ The computations were performed by fixing the axial and changing the equatorial U-O bond length.[41] However, there is an indirect influence since usually changes of the equatorial also lead to changes of the axial bond distances. There is often an inverse relation – shorter U-Oeq leads to longer U-Oax bond length. DFT + U calculations also indicate that extreme bending of uranyl can lead to smaller ΔE_{C-A} - as for example bending of the mostly linear O=U=O bond from 180° to 168.5°.[41] Note that materials with that strong bending of uranyl are very rare and specifically synthesized.[43]

The correlation between ΔE_{C-A} and the axial U-O bond length is also valid for the Np M_5 edge HR-XANES spectra of neptunyl, i.e. larger ΔE_{C-A} value corresponds to a shorter axial Np-O bond

(Table 2 and Figure 13). For example Np(VI) in perchloric acid R(Np=O) = 1.74 Å[44] has larger $\Delta E_{C\text{-}A}$ = 5.2 eV[12f] compared to $Na_2Np_2O_{7(cr)}$ with R(Np=O) = 1.76 Å,[38] $\Delta E_{C\text{-}A}$ = 3.3 eV. There is a good agreement between the $\Delta E_{C\text{-}A}$ values and axial R(Np-O_{ax}) for the **Np-cp** and the Np(V) reference; a smaller $\Delta E_{C\text{-}A}$ = 1.9 eV corresponds to longer R(Np=O) = 1.89(1) Å[45] for Np(V) compared to $\Delta E_{C\text{-}A}$ = 3.0 eV, R(Np=O) = 1.83(1) Å for **Np-cp** (Table 3). Note also that the $\Delta E_{C\text{-}A}$ correlation with the bond length depends on the oxidation state of the actinyl, but also on the coordination environment. Therefore, this analysis is most reasonable for actinyl materials with either the same An oxidation state or similar atomic environment and different oxidation states.

No intense higher energy features are observed for the $Np(IV)O_{2(am,hyd)}$ spectrum, which is the case also for the U/Pu $M_{4,5}$ edges HR-XANES spectra of U(IV) and Pu(IV) in UO_2 and PuO_2, respectively.[12d,46] In NpO_2 the Np ion has a $5f^3$ electronic configuration and cubic structure ($Fm\bar{3}m$ symmetry), therefore a different electronic structure compared to the Np(V) ($5f^2$) and Np(VI) ($5f^1$) reference compounds.

The U M_4 edge HR-XANES spectrum reveals that the oxidation state of U in **U-cp** is +VI due to its very similar energy position compared to the spectra of the **grimselite** and **metaschoepite** references (Figure 7b). The 0.1 ± 0.05 eV energy shift between peaks A of the U M_4 edge HR-XANES spectra for **grimselite**/**U-cp** and **metaschoepite** can be attributed to a higher electronic density on the U atoms in **metaschoepite**.[40] A ~0.2 eV smaller $\Delta E_{C\text{-}A}$ value is found for **grimselite** compared to **U-cp** in correlation with the slightly longer R (+ 0.02 Å, R(U=O) = 1.80 (1) Å).

DISCUSSION

We have applied the advanced spectroscopic U and Np $M_{4/5}$ edge HR-XANES technique along with conventional characterization methods to describe the coordination structure and U and Np oxidation states of Np(V) co-precipitated with U(VI) in potassium – sodium - carbonate rich

solution. The concentration of Np in the precipitate was much larger than U (< 10 % U + > 90 % Np) indicating lower solubility of the Np solid form in the given conditions (pH = 10.5, oxic conditions). The experimental and computational results as well as the thermodynamic calculations reveal that Np(V) and U(VI) alkali metal carbonate solid phases are formed. XRD, SEM-EDX, EXAFS, Np L_3 edge XANES, Raman and Np M_5 edge HR-XANES results demonstrate that $K[NpO_2CO_3]_{(cr)}$ and $K_3[NpO_2(CO_3)_2]\cdot nH_2O_{(cr)}$ are the Np phases formed. XRD reveals $K[NpO_2CO_3]_{(cr)}$, whereas EXAFS shows $K_3[NpO_2(CO_3)_2]\cdot nH_2O_{(cr)}$ as a predominant Np phase. This might be explained with higher structural disorder for the $K_3[NpO_2(CO_3)_2]\cdot nH_2O_{(cr)}$ phase. EXAFS probes the near atomic environment of U for all species, whereas XRD reveals only crystalline phases with long range atomic order.

One strong diffraction peak can be assigned to both $K_3Na[(UO_2)(CO_3)_3]\cdot H_2O_{(cr)}$ and $UO_2CO_3\cdot H_2O_{(cr)}$ phases. Due to minor differences between the U L_3 EXAFS, U L_3 XANES, U M_4 edge HR-XANES and Raman spectra for the reference $K_3Na[(UO_2)(CO_3)_3]\cdot H_2O$ and the precipitated Np(U) compound, we conclude that the $K_3Na[(UO_2)(CO_3)_3]\cdot H_2O_{(cr)}$ phase dominates, whereas the $UO_2CO_3\cdot H_2O_{(cr)}$ phase might have a small contribution.

Additional implications regarding the possible Np(V) incorporation into the U(VI) phase could be derived from Raman spectroscopy as small variations in the frequencies of Raman peaks can be a diagnostic for changes in the structure. Thus, $\nu_1(U{=}O)$ = 821 cm^{-1} is similar to pure grimselite ($K_3Na[(UO_2)(CO_3)_3]\cdot H_2O_{(cr)}$). Given the $\nu_1(Np{=}O)$ stretch in the precipitate is also very close to that reported for the neptunyl carbonates, the vibrational data corroborates two separate phases. However, the spectroscopic evidence does not allow to completely rule out incorporation of U in Np phases or Np in U phases.

Incorporation vs precipitation. The formation of separate U and Np phases in this system warrants comment. Our initial assumption is that this is primarily due to the metastability of the system and the large difference of solubility of the potassium carbonate solid phases of Np and U (lower solubility for Np(V) compared to U(VI) for the given conditions). Whilst there is precedent in the literature of actinide (in trace concentration) incorporation into the structure of uranyl minerals, we are specifically interested in what happens when high concentrations of U and Np are mixed. We note that incorporation of Np into some uranyl phases occur under mild hydrothermal approaches, either as Np(V) in a number of uranyl minerals where a charge balancing substitution occurs,[47] or a direct substitution of U(VI) for Np(VI) in metatorbernite ($Cu[(UO_2)_2(PO_4)_2].8H_2O)_{(cr)}$,[48] whilst we have postulated that Am(III) can be incorporated into the structure of grimselite.[35] The differing reactivity we observe may be due to the distinct chemical behavior and crystal chemistry of UO_2^{2+} and NpO_2^{+} carbonates.

SUMMARY

In summary we showed that Np carbonate phases with compositions close to $K[Np(V)O_2CO_3]_{(cr)}$ and $K_3[Np(V)O_2(CO_3)_2]\cdot nH_2O_{(cr)}$ co-precipitated from aqueous K-Na-U(VI)-CO_3-H_2O systems along with the minor $K_3Na[(U(VI)O_2)(CO_3)_3]_{(cr)}$ phase. Small contribution of $U/VI)O_2CO_3\cdot H_2O_{(cr)}$ could not be excluded. We did not find clear evidence for incorporation of U/Np in Np/U crystalline/amorphous phases. The thermodynamic calculations suggest that $K_3Na[(UO_2)(CO_3)_3]_{(cr)}$ and $K_3[NpO_2(CO_3)_2]\cdot nH_2O_{(cr)}$ should be formed, so it might be that in the short timescales of these experiments, the system did not reach thermodynamic equilibrium. However, given the uncertainties in the thermodynamic data available, the modelling results should not be over-interpreted. Np 3d4f RIXS and M_5 edge HR-XANES was applied for oxidation state and coordination studies of Np for the first time. The correlation between the size of the

energy shift of peak C compared to peak A (ΔE_{C-A}) in Np M_5 edge HR-XANES spectra and the axial Np-O bond lengths for neptunyl(V)/(VI) was demonstrated. The observation that Np(V) carbonates precipitate in preference to uranyl carbonates in alkaline K-Na-U(VI)-CO_3-H_2O systems is important for understanding the fundamental chemical behavior of actinides in a potassium carbonate rich aqueous system.

ASSOCIATED CONTENT

Supporting Information: Sample holder for An $M_{4,5}$ edges HR-XANES, SEM images of the precipitate, Np L_3 edge EXAFS spectra of **Np-cp** fitted with two and three shells; Computed U and Np L_3 edge XANES spectra and an input file for the FDMNES calculations.

AUTHOR INFORMATION

*Corresponding Authors

*E-mail: tonya.vitova@kit.edu; Tel: +49-721-608-24024

*E-mail: bakerrj@tcd.ie; Tel: +353-1-8963501

AUTHOR CONTRIBUTIONS

The manuscript was written through contributions of all authors. All authors have given approval to the final version of the manuscript.

ACKNOWLEDGMENTS

RJB and TV thank TALISMAN for funding this work. The authors acknowledge the Helmholtz Association of German Research Centers for the VH-NG-734 grant. V.M acknowledges the German Federal Ministry of Education and Research (BMBF, grant agreement 02NUK053A) and

the Initiative and Networking Fund of the Helmholtz Association (HGF grant SO-093) within the iCross for partial funding. We acknowledge the Karlsruhe research accelerator (KARA) (previous ANKA) for the provided beamtime. IP thanks Dr. Evgeny Blokhin (Tilde Material Informatics) for providing the crystal structures of the K-Np-CO_3 compounds.

535 FIGURES

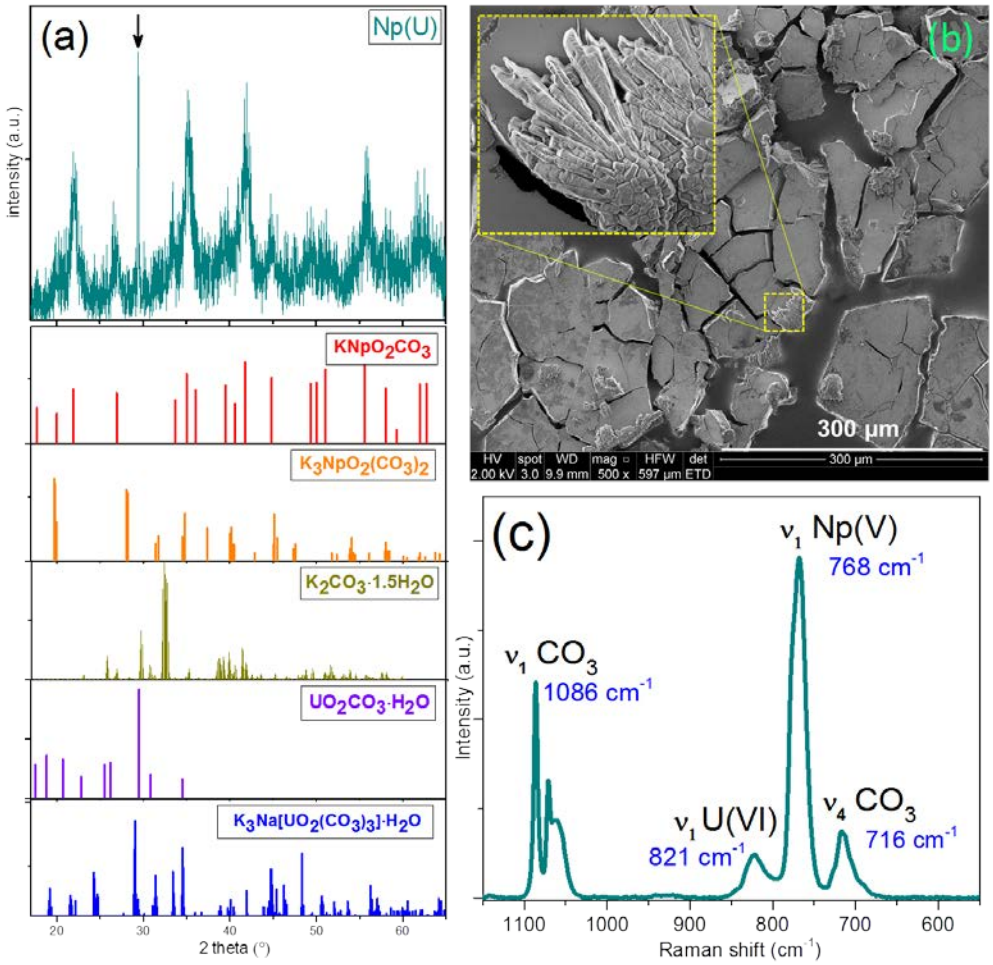

Figure 1. (a) pXRD pattern of Np(U) precipitate (top) with pXRD patterns of $K[NpO_2CO_3]_{(cr)}$ (Bruker PDF 170264 based on 32a), $K_3[NpO_2(CO_3)_2]_{(cr)}$ (reproduced from Volkov et al.),[21] $K_2CO_3 \cdot 1.5H_2O$ (ISCD 22257), rutherfordine ($UO_2CO_3 \cdot H_2O_{(cr)}$) (reproduced from Finch et al.)[34] and grimselite ($K_3Na[UO_2(CO_3)_3] \cdot H_2O_{(cr)}$) (as measured with Bruker AXS D8 – it agrees with AMCSD 0005731), peak from possibly U phase is indicated by a black arrow; (b) SEM images of the Np(U) precipitate and K_2CO_3 crystals formed on a cracked Np(U) precipitate after drying and preparation for SEM analysis (K_2CO_3 crystals are identified by the zoomed in regions); (c) Raman spectrum of Np(U) precipitate.

536

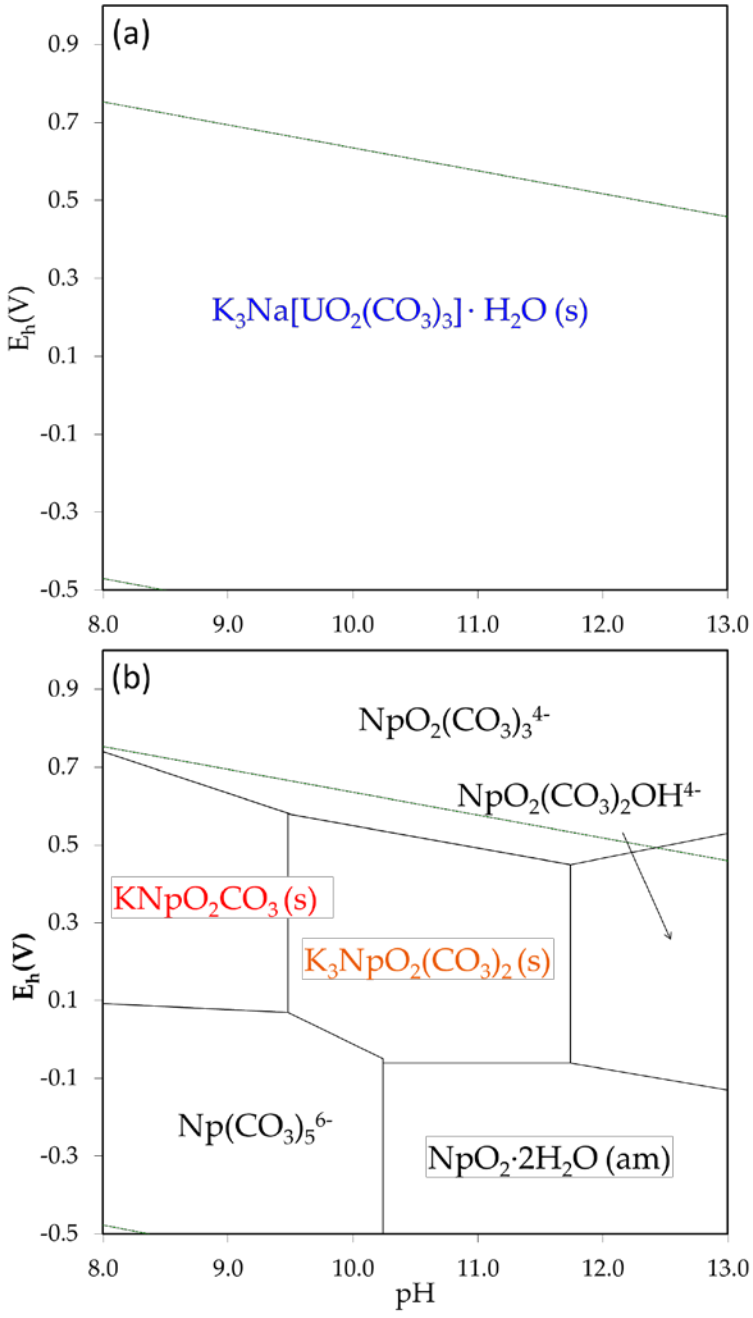
(a)
0.9
0.7
0.5
0.3
0.1
-0.1
-0.3
-0.5
E_h(V)
K3Na[UO2(CO3)3]· H2O (s)
8.0
9.0
10.0
11.0
12.0
13.0
(b)
NpO2(CO3)3 4-
NpO2(CO3)2OH4-
KNpO2CO3 (s)
K3NpO2(CO3)2 (s)
Np(CO3)5 6-
NpO2·2H2O (am)
pH

Figure 2. (a) U and (b) Np Pourbaix diagrams: $[U]_{TOT} = 9.9 \cdot 10^{-3}$ M, $[Np]_{TOT} = 8.4 \cdot 10^{-5}$ M, Na_2CO_3 ([Na] = 0.24 M), K_2CO_3 ([K] = 0.74 M), $[CO_3]_{TOT}$ = 0.49 M. The expected phases are given with colors.

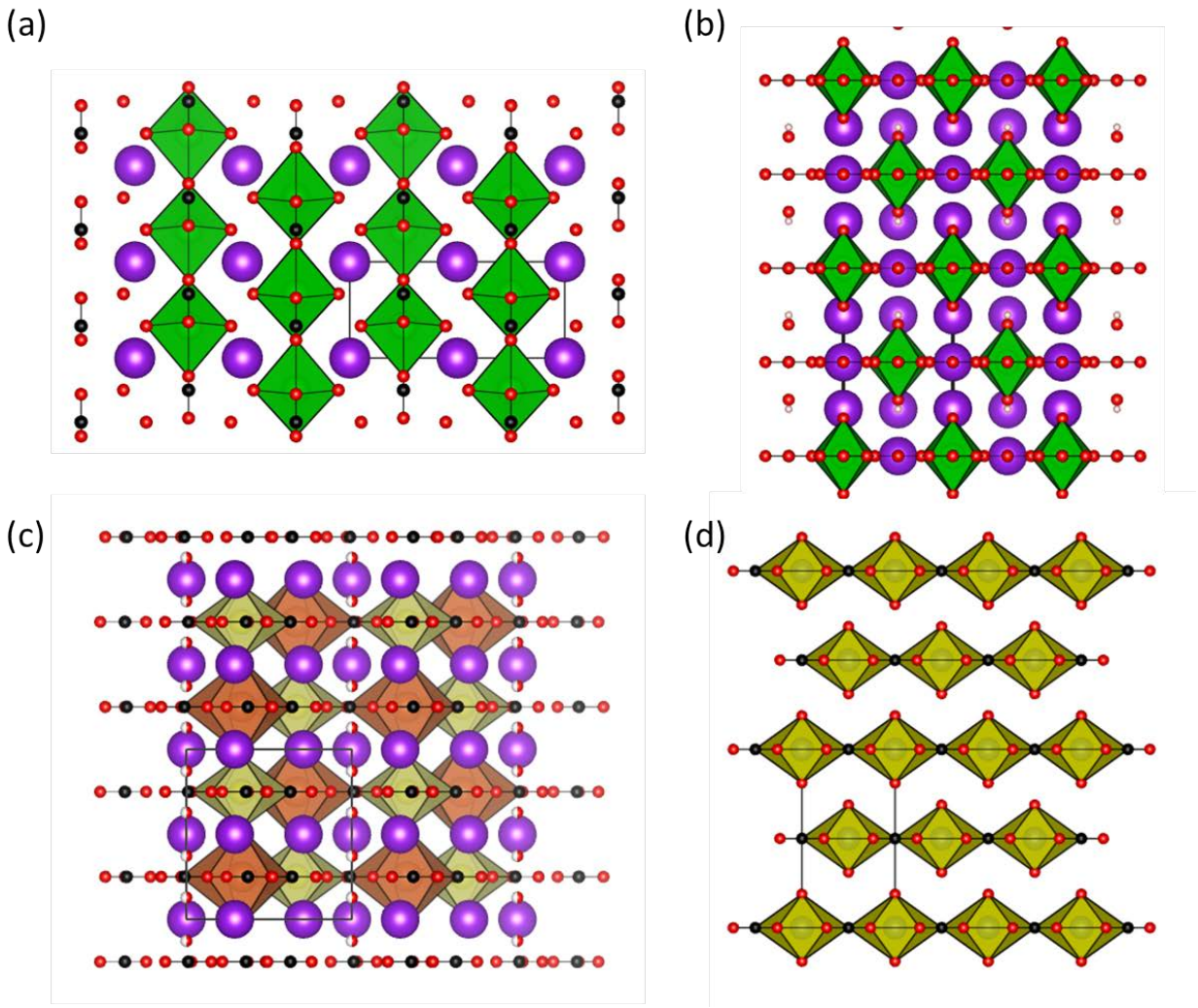

Figure 3. Structures of (a) $K[NpO_2CO_3]_{(cr)}$; (b) $K_3[NpO_2(CO_3)_2]_{(cr)}$; (c) **grimselite** ($K_3Na[UO_2(CO_3)_3]\cdot H_2O_{(cr)}$) and (d) **rutherfordine** ($UO_2CO_3\cdot H_2O_{(cr)}$) showing the different

layer structures. Key: Np – green polyhedral; U – yellow polyhedral, Na – orange; K – purple; O – red; C – black.

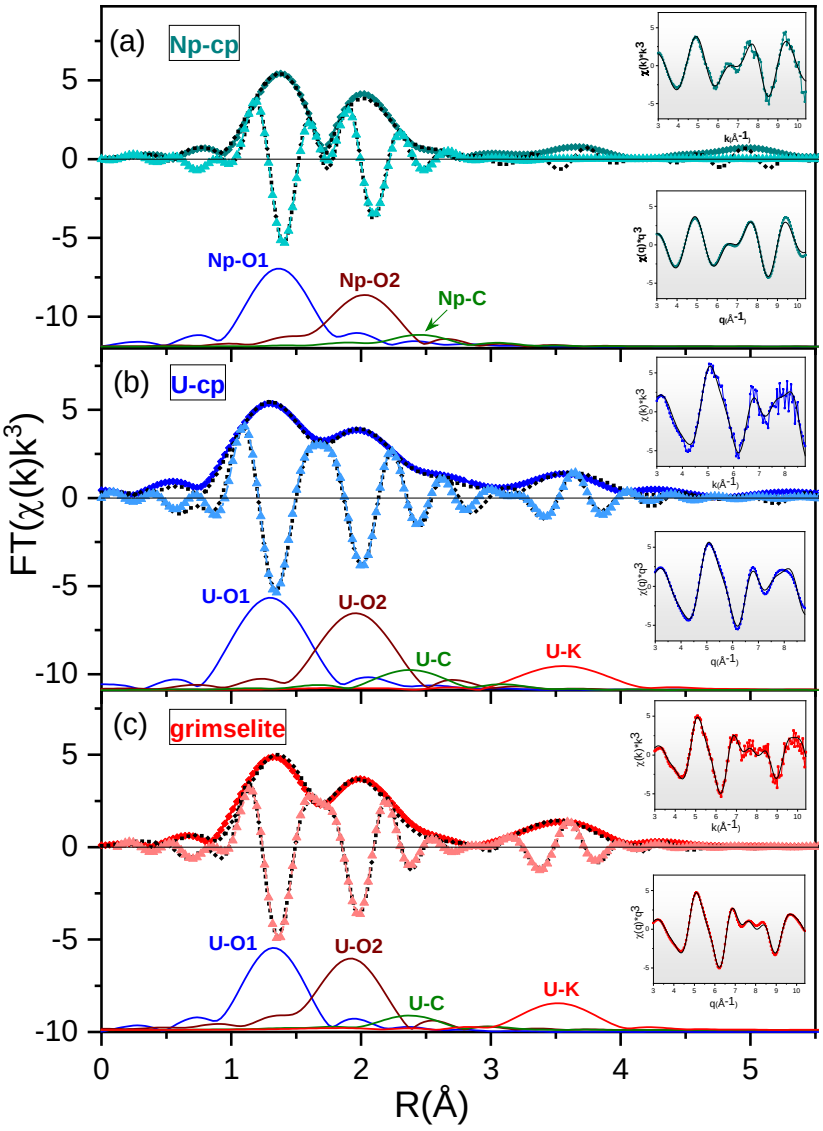

537

Figure 4. (a) R-space fit results for the **Np-cp**, (b) **U-cp** and (c) **grimselite** magnitude of the FT-EXAFS (colored rhombs) and their best fits (black dash dot line) and single scattering paths; imaginary parts of the FT-EXAFS (light colored triangles) and the best fits (black dash line) (top

inset); k^3-weighted filtered $\chi(k)$-function (colored rhombs) and their best fits (black solid line); back-transformed EXAFS and the back-transformed fits (bottom inset).

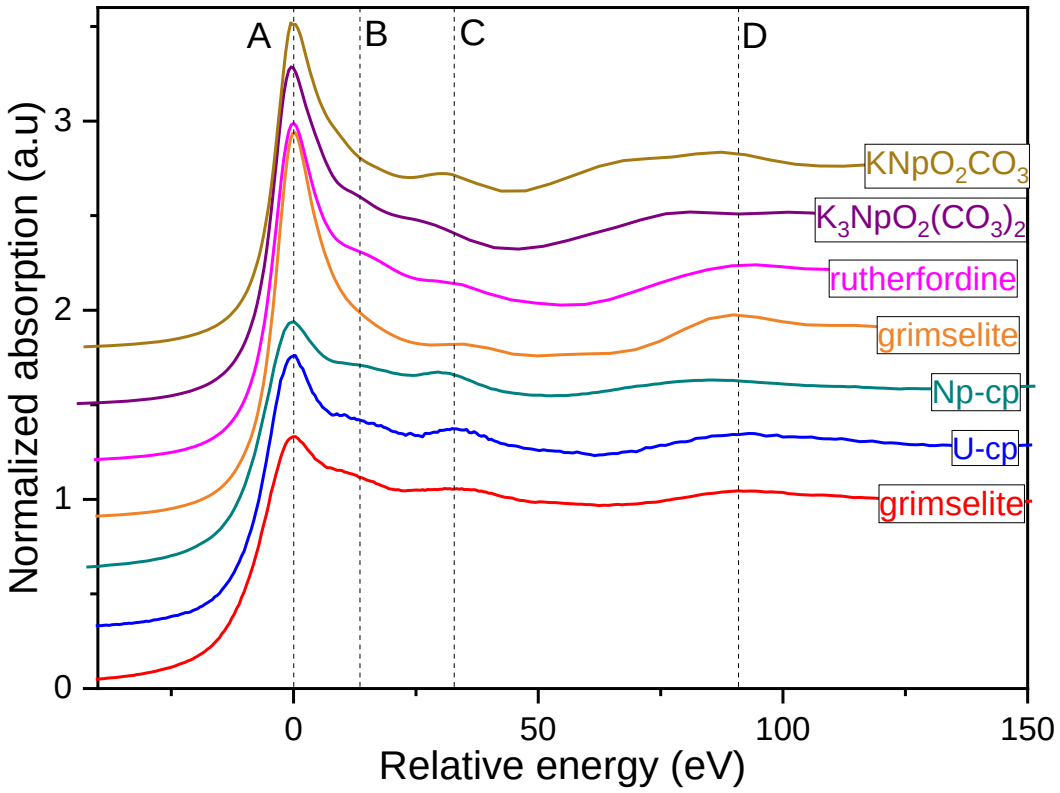

Figure 5. From bottom to top: experimental U L_3 edge XANES spectra of **grimselite, U-cp** and Np L_3 edge XANES spectrum of the **Np-cp** samples. U L_3 edge XANES of **grimselite** ($K_3Na[UO_2(CO_3)_3]\cdot H_2O_{(cr)}$), **rutherfordine** ($UO_2CO_3\cdot H_2O_{(cr)}$) and Np L_3 edge XANES of $K_3[NpO_2(CO_3)_2]_{(cr)}$, and $K[NpO_2CO_3]_{(cr)}$ computed with the FDMNES code. All spectra are aligned and plotted on a relative energy scale so that the most intense peak is at 0 eV.

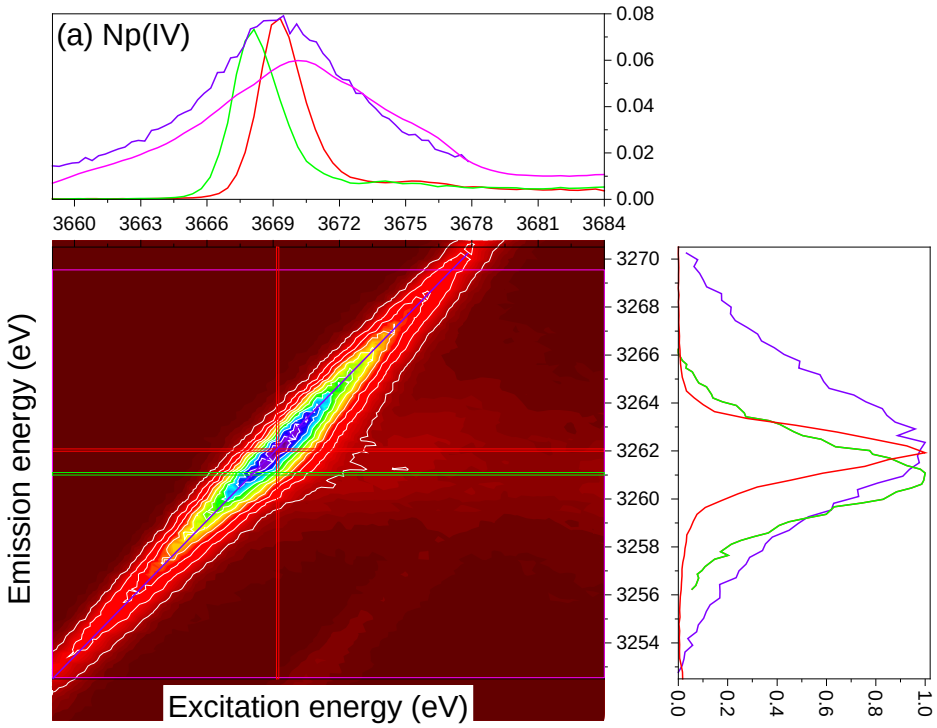
(a) Np(IV)
0.08
0.06
0.04
0.02
0.00
3660
3663
3666
3669
3672
3675
3678
3681
3684
3270
3268
3266
3264
3262
3260
3258
3256
3254
Emission energy (eV)
Excitation energy (eV)
0.0
0.2
0.4
0.6
0.8
1.0

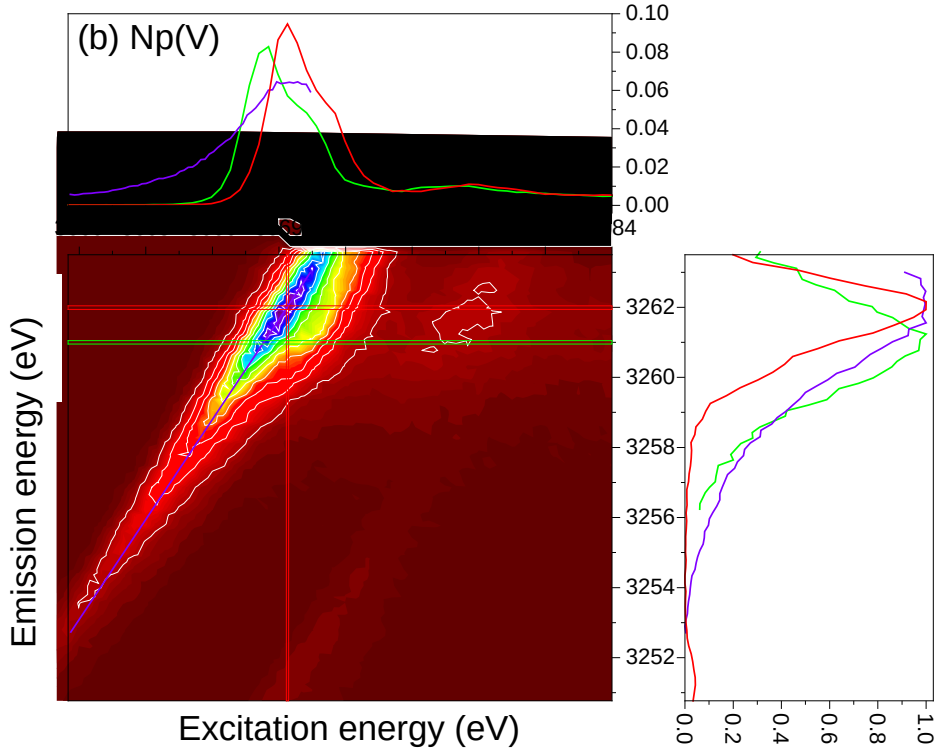
(b) Np(V)
0.10
0.08
0.06
0.04
0.02
0.00
3262
3260
3258
3256
3254
3252
Emission energy (eV)
Excitation energy (eV)
0.0
0.2
0.4
0.6
0.8
1.0

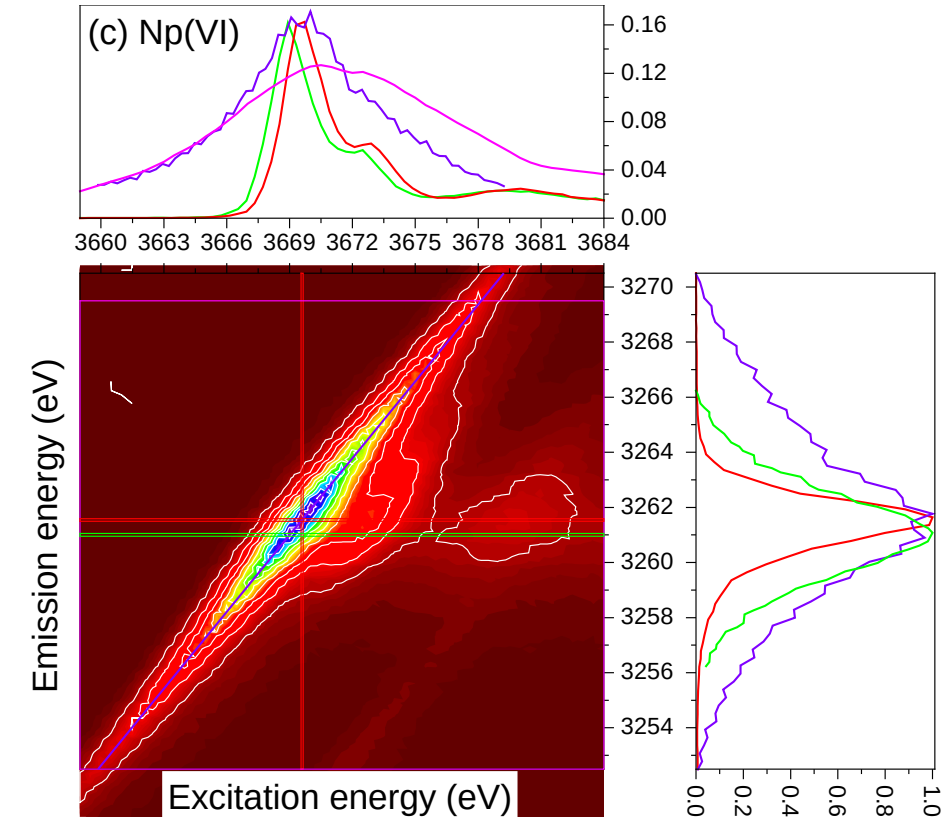
(c) Np(VI)
0.16
0.12
0.08
0.04
0.00
3660 3663 3666 3669 3672 3675 3678 3681 3684
Emission energy (eV)
3270
3268
3266
3264
3262
3260
3258
3256
3254
Excitation energy (eV)
0.0 0.2 0.4 0.6 0.8 1.0

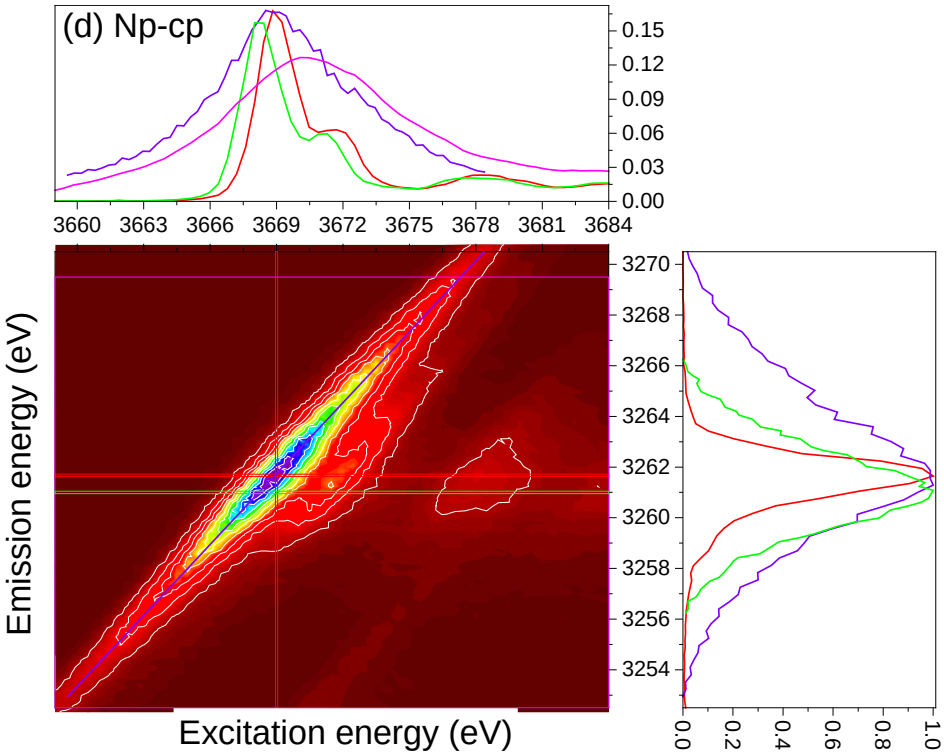
(d) Np-cp
0.15
0.12
0.09
0.06
0.03
0.00
3660 3663 3666 3669 3672 3675 3678 3681 3684
Emission energy (eV)
3270
3268
3266
3264
3262
3260
3258
3256
3254
Excitation energy (eV)
0.0 0.2 0.4 0.6 0.8 1.0

Figure 6. (a) Np 3d4f RIXS maps of $Np(IV)O_{2(am,hyd)}$, (b) $Ca_{0.5}Np(V)O_2(OH)_2 \cdot 1.3H_2O_{(cr)}$, (c) $Na_2Np(VI)_2O_{7(cr)}$ and (d) **Np-cp**. The energy positions of the maxima of the normal (measured 3700 eV excitation energy) and resonant emission lines are marked with horizontal green and red lines, respectively. Those lines are shown in green and red (obtained at the position of the red vertical line) lines on the right side of the maps. The violet line marks the cross section of the most intense resonance in the RIXS map. The cross sections plotted along the emission and the excitation energy scales are shown also with violet lines on the right and top of the RIXS maps, respectively. Rectangle in magenta with 17 eV width shows the emission energy region over which the intensity is integrated to obtain the conventional Np M_5 edge XANES spectrum plotted on the top also in magenta. The intensity of this spectrum is multiplied by 5.

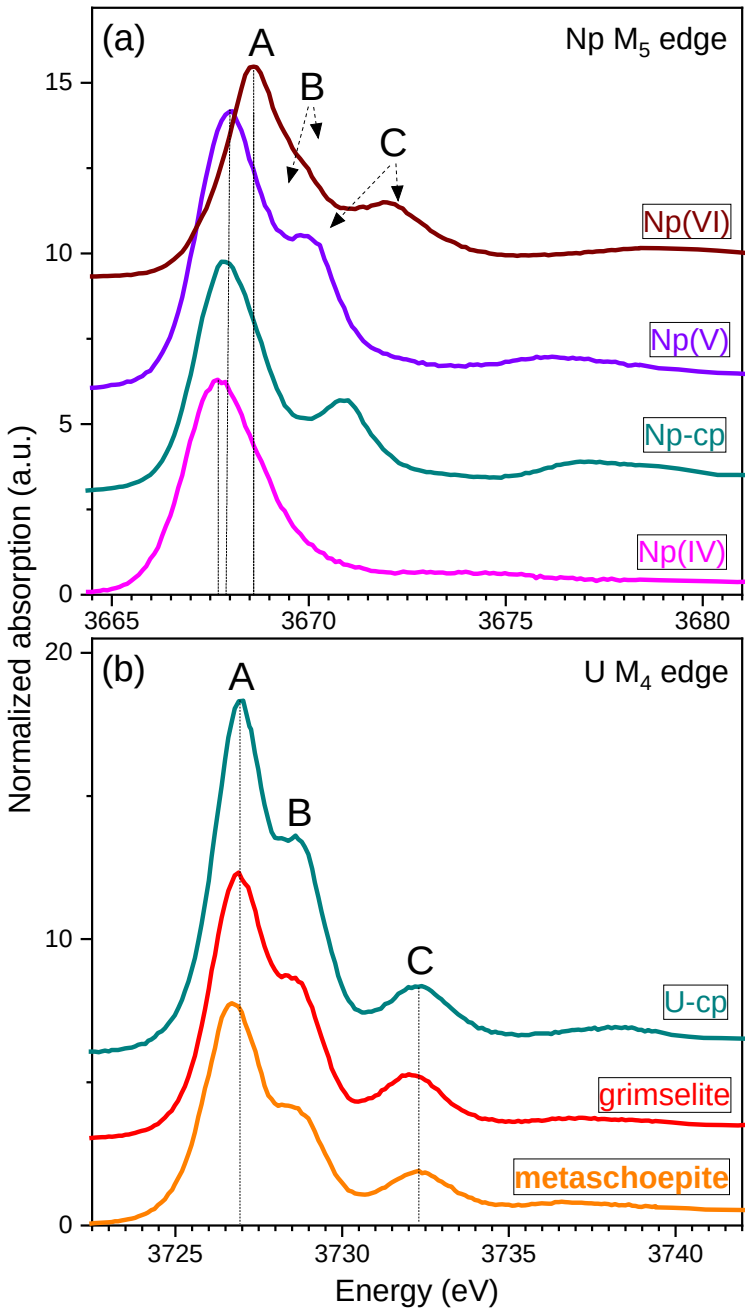

Figure 7. (a) From top to bottom: Np M_5 edge HR-XANES spectra of $Na_2Np(VI)_2O_{7(cr)}$, $Ca_{0.5}Np(V)O_2(OH)_2 \cdot 1.3H_2O_{(cr)}$, **Np-cp** and $Np(IV)O_{2(am,hyd)}$. (b) U M_4 edge HR-XANES spectra of **U-cp**, **grimselite** and **metaschoepite**.

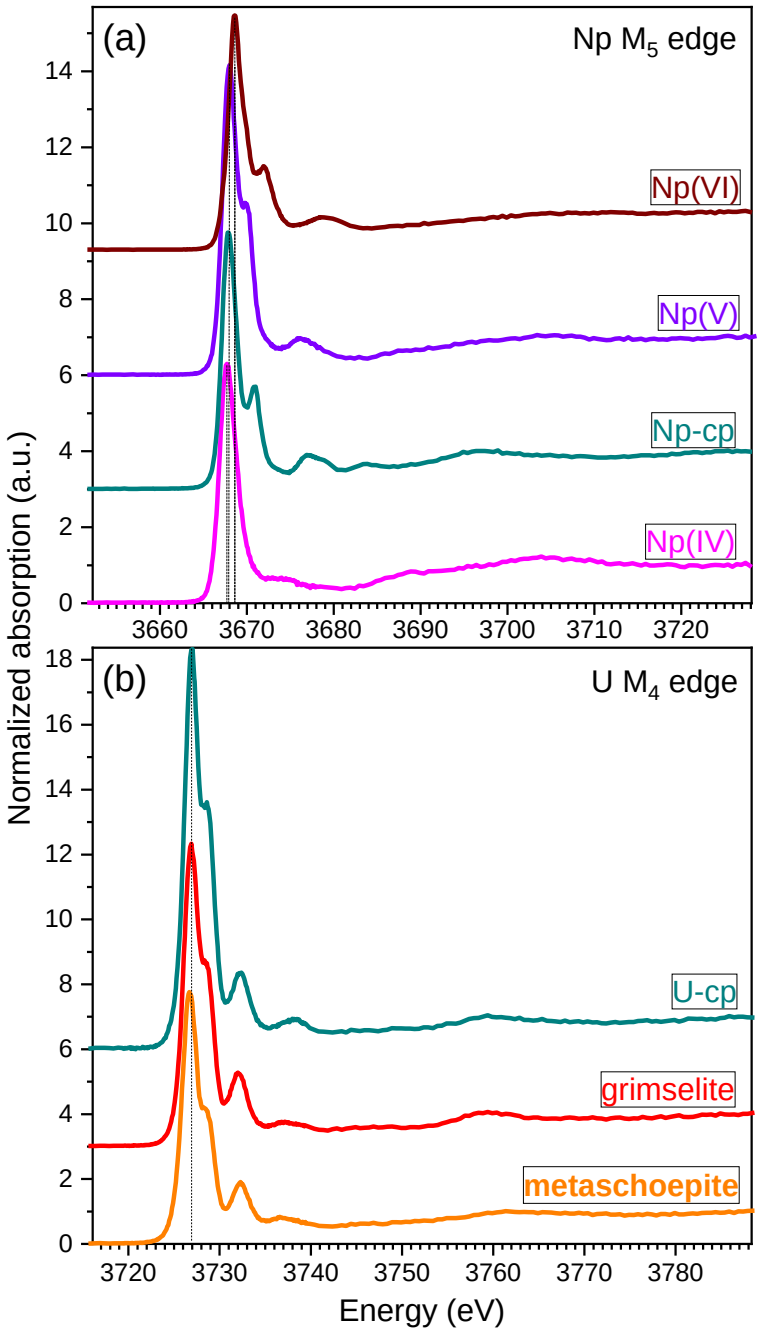

Figure 8. (a) From top to bottom: Np M_5 edge HR-XANES spectra of $Na_2Np(VI)_2O_{7(cr)}$, $Ca_{0.5}Np(V)O_2(OH)_2 \cdot 1.3H_2O_{(cr)}$, **Np-cp** and $Np(IV)O_{2(am,hyd)}$. (b) U M_4 edge HR-XANES spectra of **U-cp**, **grimselite** and **metaschoepite**.

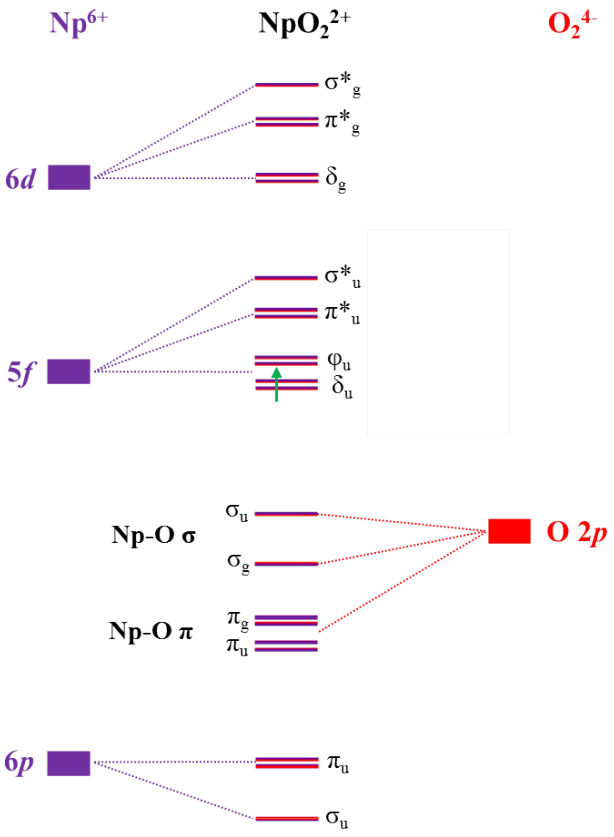

Figure 9 A qualitative molecular orbital scheme of neptunyl adapted from 49. Only frontier electrons are indicated.

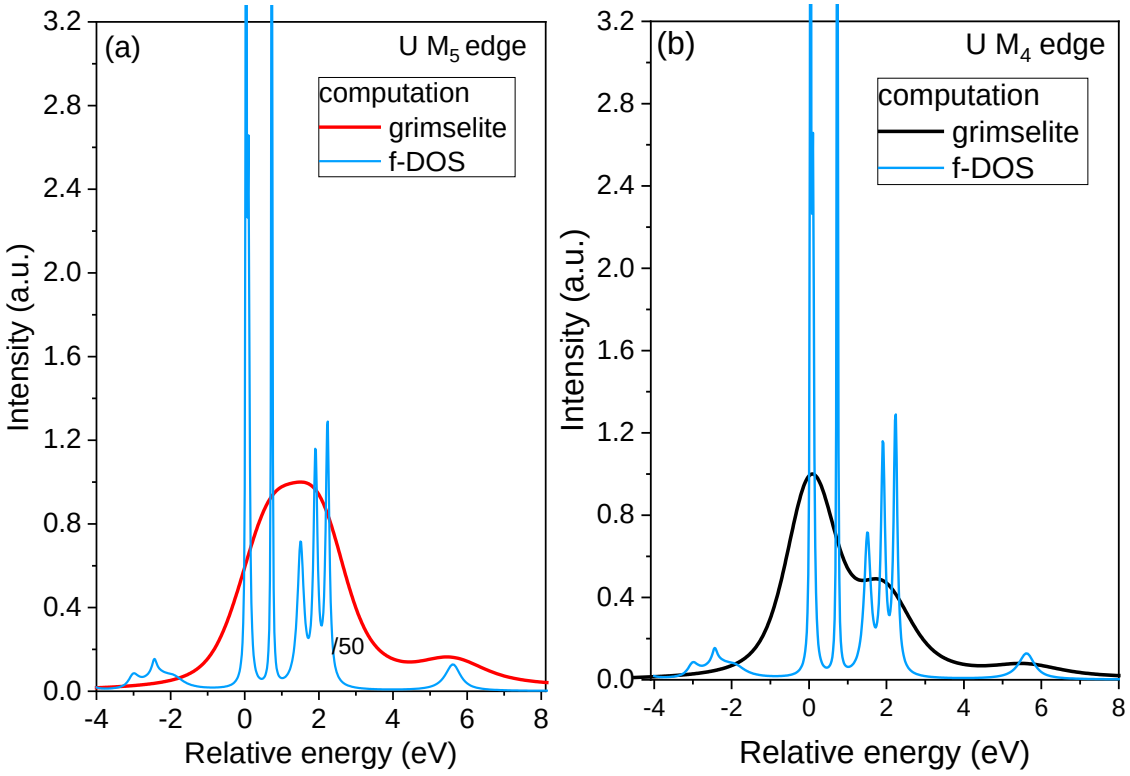

538
539

540 Figure 10. (a) U M_5 and (b) M_4 edge HR-XANES spectra and f-DOS of **grimselite**

541 ($K_3Na[UO_2(CO_3)_3]\cdot H_2O_{(cr)}$) computed with the FDMNES code.

542

543

544

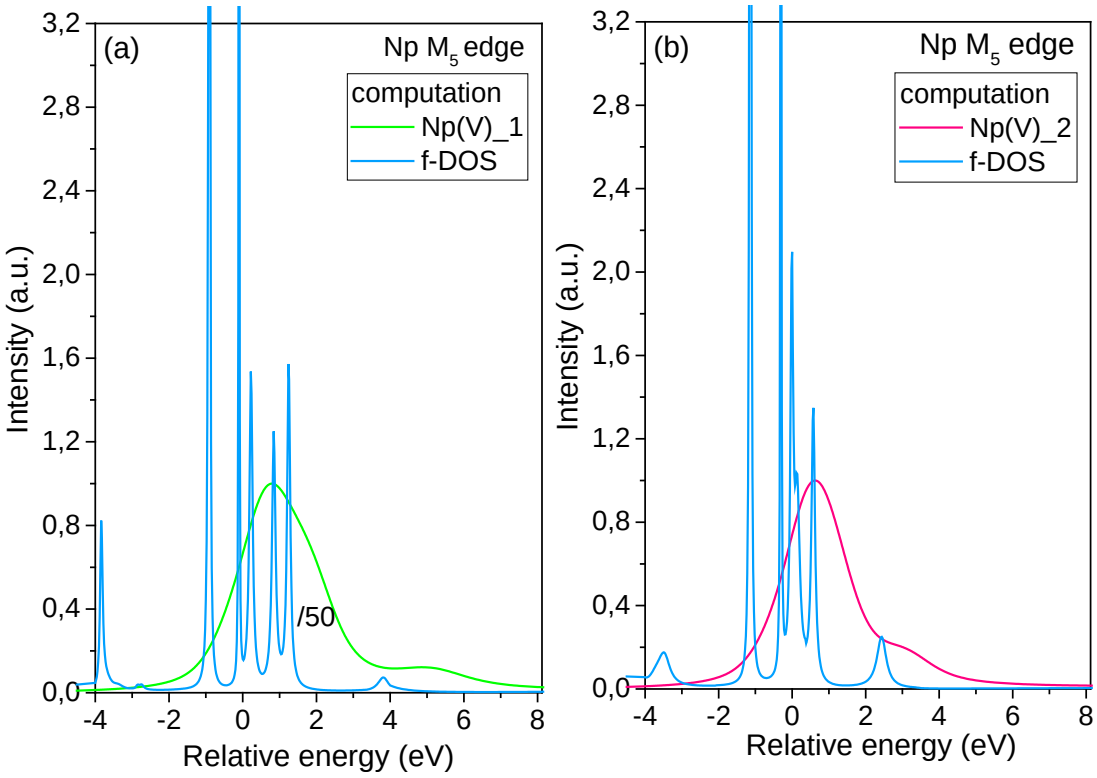

Figure 11. Np M_5 edge HR-XANES spectra and f-DOS of (a) $K_3[NpO_2(CO_3)_2]\cdot nH_2O$(cr) (Np(V)_1), and (b) $K[NpO_2CO_3]$(cr) (Np(V)_2) computed with the FDMNES code.

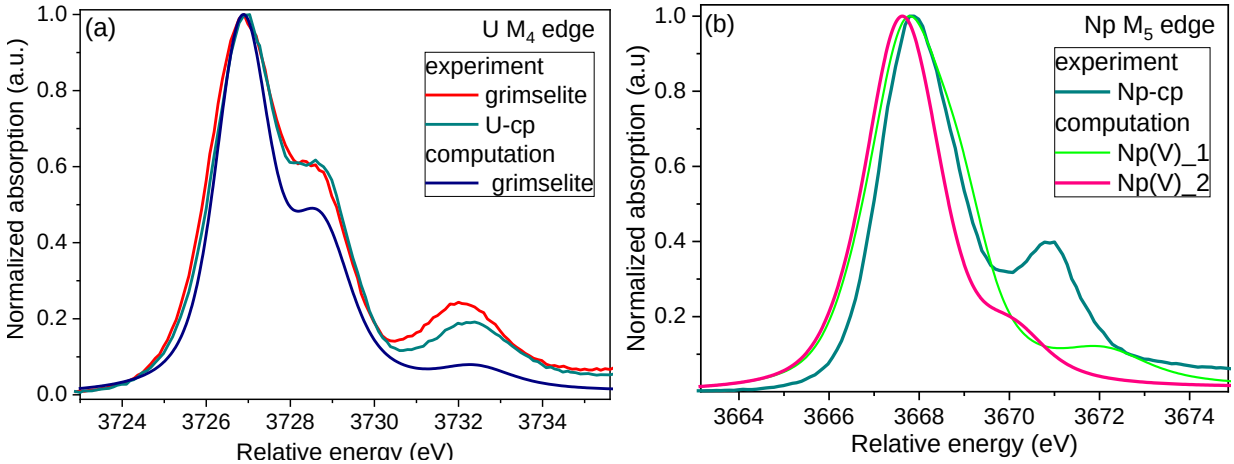

Figure 12. (a) U M_4 edge HR-XANES spectra of **grimselite** ($K_3Na[UO_2(CO_3)_3]\cdot H_2O_{(cr)}$), **U-cp** and a computed spectrum of **grimselite**. (b) Np M_5 edge HR-XANES spectra of **Np-cp** and

555 computed spectra of $K_3[NpO_2(CO_3)_2]\cdot nH_2O$(cr), and $K[NpO_2CO_3]$(cr). The computations are

556 performed with the FDMNES code.

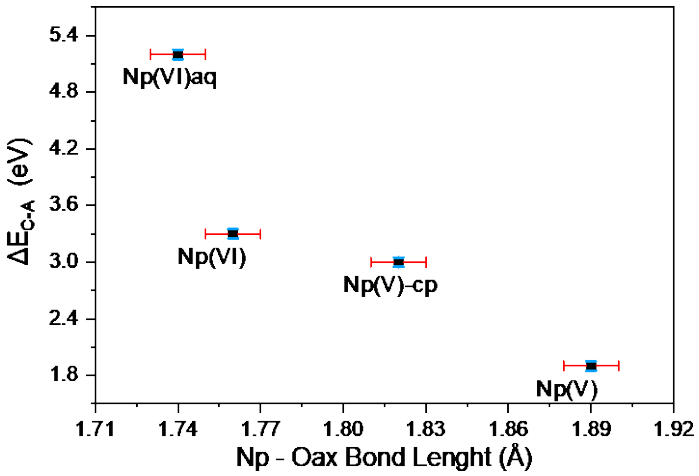

557

558 Figure 13. Correlation between the energy shift between peaks A and C of the Np M_5 edge HR-

559 XANES spectra of neptunyl(V)/(VI) compounds (cf. Figure 7a) as a function of the Np – O axial

560 bond length (cf. Table 3). The Np(VI)aq – Np in perchloric acid,[12f] Np(V) -

561 $Ca_{0.5}Np(V)O_2(OH)_2\cdot 1.3H_2O_{(cr)}$, Np(VI) - $Na_2Np(VI)_2O_{7(cr)}$ and **Np(V)-cp**.

562

563

564

565

566

567

568

TABLES

Table 1. EXAFS fit results for the **Np-cp**, **U-cp** and **grimselite** (SP denotes scattering path, N – coordination number, R – interatomic distance, σ^2 - Debye-Waller factor, ΔE_0 – energy shift of the ionization potential, r - goodness of fit parameter. The S_0^2 – amplitude reduction factor is fixed to 0.8. Uncertainties are given in the parentheses as the last decimal in the fit value, ^{f} – parameters are fixed). The O coordination number in the Np – O1 scattering path was first fixed to 2. As a second step N and R were consecutively varied until the best fit was obtained.

Sample	SP	N	R, [Å]	$\sigma^2 \cdot 10^{-3}$, [Å^2]	ΔE_0, [eV]	r, %
Np-cp	Np-O1	2^f	1.83 (1)	0.8 (7)	7.4 (11)	0.5
(Np in Np(U)	Np-O2	5.4 (4)	2.53 (1)	6 (1)		
precipitate	Np-C	2.9 (10)	2.99 (4)	6 (1)		
U-cp	U-O1	2.4^f	1.78 (1)	1.0 (9)	4.3 (4)	0.4
(U in Np(U)	U-O2	5.9 (5)	2.44 (1)	4 (1)		
precipitate)	U-C	3.5 (4)	2.91 (2)	4 (1)		
	U-K	5.0 (18)	4.02 (2)	8 (3)		
Grimselite	U-O1	2^f	1.80 (1)	2 (1)	3.2 (8)	0.7
(reference)	U-O2	5.3 (5)	2.41 (1)	6 (1)		
	U-C	2.7 (7)	2.90 (2)	6 (1)		
	U-K	5.1 ± 1.9	3.98 (3)	7 (2)		

Table 2. U/Np-O and U/Np-C interatomic distances for the O and C atoms in the first and second coordination spheres of U and Np in reference solid compounds proposed by XRD to be present in the Np(U) precipitate.

Solid compound	R(U-O)ax, Å	R(U-O)eq, Å	R(U-C), Å
$K_3[NpO_2(CO_3)_2]\cdot nH_2O_{(cr)}$ Volkov et al.[21]	1.80	2.58	*
$K[NpO_2CO_3]_{(cr)}$ ICSD 15685	1.96	2.57	2.96
grimselite $K_3Na[UO_2(CO_3)_3]\cdot H_2O_{(cr)}$) AMCSD 0005731	1.78	2.42	2.89
rutherfordine $UO_2CO_3\cdot H_2O_{(cr)}$ ICSD 87760	1.74	2.44-2.52	2.94

*The U-C value is not reported in the Ref. 21

Table 3. Energy positions of spectral peaks and energy differences for the Np/U M_5/M_4 edge HR-XANES spectra of Np(VI), Np(V), **Np-cp**, Np(IV) and **U-cp**, **grimselite** (AMCSD 0005731), **metaschoepite** (AMCSD 0004319) depicted in Figure 7. The uncertainty of the energy positions is ± 0.05 eV. The R(An=O) bond lengths are found from EXAFS (cf. Table 1) - *X. Gaona et al.[38] and & D. Fellhauer.[45]

Sample	**A [eV]**	**B [eV]**	**C [eV]**	**B-A [eV]**	**C-A [eV]**	**R(An-O)ax [Å], ± 0.01**
Np(VI) ($Na_2Np_2O_{7(cr)}$)	3668.6	-	3671.9	-	3.3	1.76*
Np(V) ($Ca_{0.5}NpO_2(OH)_2 \cdot 1.3H_2O_{(s)}$)	3668.0	-	3669.9	-	1.9	1.89&
Np-cp (Np in Np(U) precipitate)	3667.9	-	3670.9	-	3.0	1.83
Np(IV) ($NpO_{2(am,hyd)}$)	3667.7	-	-	-	-	-
U-cp (U in Np(U) precipitate)	3726.9	3728.6	3732.3	1.7	5.4	1.78
grimselite ($K_3Na[UO_2(CO_3)_3] \cdot H_2O$)	3726.9	3728.6	3732.1	1.7	5.2	1.80
metaschoepite ($[(UO_2)_4O(OH)_6] \cdot 5H_2O$)	3726.7	3728.5	3732.3	1.8	5.6	1.77

CURRENT AFFILIATION:

Dr. Vanessa Montoya

Department of Environmental Informatics, Helmholtz Centre for Environmental Research – UFZ, Permoserstr. 15, 04318, Leipzig, Germany

569 REFERENCES

[1] (a) Arai, Y.; Moran, P. B.; Honeyman, B. D.; Davis, J. A. In situ spectroscopic evidence for neptunium(V)-carbonate inner-sphere and outer-sphere ternary surface complexes on hematite surfaces. *Environ. Sci. Technol.* 2007, *41*, 3940-3944; (b) Clark, D. L.; Conradson, S. D.; Ekberg, S. A.; Hess, N. J.; Janecky, D. R.; Neu, M. P.; Palmer, P. D.; Tait, C. D. A multi-method approach to actinide speciation applied to pentavalent neptunium carbonate complexation. *New J. Chem.* 1996, *20*. 211-220; (c) Clark, D. L.; Conradson, S. D.; Ekberg, S. A.; Hess, N. J.; Neu, M. P.; Palmer, P. D.; Runde, W.; Tait, C. D. EXAFS studies of pentavalent neptunium carbonato complexes. Structural elucidation of the principal constituents of neptunium in groundwater environments. *J. Am. Chem. Soc.* 1996, *118*, 2089-2090; (d) Madic, C.; Hobart, D. E.; Begun, G. M. Raman spectrometric studies of actinide(V) and -(VI) complexes in aqueous sodium carbonate solution and of solid sodium actinide(V) carbonate compounds. *Inorg. Chem.* 1983, 22, 1494-1503; (e) Rai, D.; Hess, N. J.; Felmy, A. R.; Moore, D. A.; Yui, M. A Thermodynamic model for the solubility of NpO_2(am) in the aqueous K^+-HCO_3^--CO_3^{2-}-OH-H_2O system. *Radiochim. Acta* 1999, 84. 159-169.

[2] Ikeda-Ohno, A.; Tsushima, S.; Takao, K.; Rossberg, A.; Funke, H.; Scheinost, A. C.; Bernhard, G.; Yaita, T.; Hennig, C. Neptunium carbonato complexes in aqueous solution: An

electrochemical, spectroscopic, and quantum chemical study. *Inorg. Chem.* 2009, 48, 11779-11787.

[3] Balboni, E.; Morrison, J. M.; Wang, Z.; Engelhard, M. H.; Burns, P. C. Incorporation of Np(V) and U(VI) in carbonate and sulfate minerals crystallized from aqueous solution. *Geochim. Cosmochim. Acta* 2015, *151*. 133-149.

[4] Heberling, F.; Denecke, M. A.; Bosbach, D., Neptunium(V) coprecipitation with calcite. *Environ. Sci. Technol.* 2008, 42, 471-476.

[5] (a) Smith, K.F.; Bryan, N.D.; Law, G.T.W.; Hibberd, R.; Shaw, S.; Livens, F.R.; Parry, S.A.; Mosselmans J. F. W.; Morris, K. D. Np(V) sorption and solubility in high pH calcite systems. *Chem. Geol.* 2018, *493*, 396-404; (b) Heberling, F.; Brendeback, B.; Bosbach, D. Neptunium(V) adsorption to calcite. *J. Contam Hydrol.*, 2008, *102*, 246-252.

[6] (a) Nakata, K.; Nagasaki, S.; Tanaka, S.; Sakamoto, Y.; Tanaka, T.; Ogawa, H. Sorption and reduction of neptunium(V) on the surface of iron oxides. *Radiochim. Acta* 2002, 90, 665−669; (b) Nakata, K.; Nagasaki, S.; Tanaka, S.; Sakamoto, Y.; Tanaka, T.; Ogawa, H. Reduction rate of neptunium(V) in heterogeneous solution with magnetite. *Radiochim. Acta* 2004, *92*, 145−149; (c) Moyes, L. N.; Jones, M. J.; Reed, W. A.; Livens, F. R.; Charnock, J. M.; Mosselmans, J. F. W.; Hennig, C.; Vaughan, D. J.; Pattrick, R. A. D. An X-ray absorption spectroscopy study of neptunium(V) reactions with mackinawite (FeS). *Environ. Sci. Technol.* 2002, *36*, 179−183; (d) Christiansen, B. C.; Geckeis, H.; Marquardt, C. M.; Bauer, A.; Römer, J.; Wiss, T.; Schild, D.; Stipp, S. L. S. Neptunyl (NpO2+) interaction with green rust, GR(Na,SO4). *Geochim. Cosmochim. Acta* 2011, *75*, 1216−1226; (e) Fröhlich, D. R.; Amayri, S.; Drebert, J.; Grolimund, D.; Huth, J.; Kaplan, U.; Krause, J.; Reich, T. Speciation of Np(V) uptake by Opalinus Clay using synchrotron

microbeam techniques. *Anal. Bioanal. Chem.* 2012, *404*, 2151−2162; (f) Brookshaw, D. R.; Pattrick, R. A. D.; Bots, P.; Law, G. T. W.; Lloyd, J. R.; Mosselmans, J. F. W.; Vaughan, D. J.; Dardenne, K.; Morrie, K. Redox Interactions of Tc(VII), U(VI), and Np(V) with Microbially Reduced Biotite and Chlorite. *Environ. Sci. Technol*. 2015, *49*, 13139−13148; (g) Wylie, E. M.; Olive, D. T.; Powell, B. A. Effects of Titanium Doping in Titanomagnetite on Neptunium Sorption and Speciation. *Environ. Sci. Technol.* 2016, *50*, 1853−1858.

[7] Scheinost, A.C.; Steudtner, R.; Hübner, R.; Weiss, S.; Bok, F. Neptunium^{V} Retention by Siderite under Anoxic Conditions: Precipitation of NpO_2–Like Nanoparticles and of Np^{IV} Pentacarbonate. *Environ. Sci. Technol*. 2016, *50*, 10413-10420.

[8] (a) Burns, P. C.; Ewing, R. C.; Navrotsky, A. Nuclear fuel in a reactor accident. *Science* 2012, *335*. 1184-1188; (b) Burakov, B. E.; Strykanova, E. E.; Anderson, E. B. Secondary uranium minerals on the surface of Chernobyl "lava" *Mater. Res. Soc. Symp. Proc.* 1997, *465*, 1309-1311.

[9] Burns, P. C.; Finch, R. J. Wyartite: Crystallographic evidence for the first pentavalent-uranium mineral. *Am. Mineral*. 1999, *84*, 1456-1460.

[10] Baker, R. J. Uranium minerals and their relevance to long term storage of nuclear fuels. *Coord. Chem. Rev.* 2014, *266-267*, 123-136.

[11] Meredith, N. A.; Sigmon, G. E.; Simonetti, A.; Burns P. C. Structural and Morphological Influences on Neptunium Incorporation in Uranyl Molybdates. *Crystal Growth & Design*, 2015, *15*, 5293-5300.

[12] (a) Vitova, T.; Denecke, M. A.; Göttlicher, J.; Jorissen, K.; Kas, J. J.; Kvashnina, K.; Prüßmann, T.; Rehr, J. J.; Rothe, J. Actinide and lanthanide speciation with high-energy resolution X-ray

techniques. *J. Phys*. 2013, *430*, 012117; (b) Kvashnina, K. O.; Butorin, S. M.; Martin, P.; Glatzel, P. Chemical State of Complex Uranium Oxides. *Phys Rev Lett* 2013, *111*, 253002; (c) Pidchenko, I.; Kvashnina, K. O.; Yokosawa, T.; Finck, N.; Bahl, S.; Schild, D.; Polly, R.; Bohnert, E.; Rossberg, A.; Göttlicher, J.; Dardenne, K.; Rothe, J.; Schäfer, T.; Geckeis, H.; Vitova, T., Uranium Redox Transformations after U(VI) Coprecipitation with Magnetite Nanoparticles. *Environ. Sci. Technol.* 2017, *51*, 2217-2225; (d) Popa, K.; Prieur, D.; Manara, D.; Naji, M.; Vigier, J. F.; Martin, P. M.; Blanco, O. D.; Scheinost, A. C.; Prussmann, T.; Vitova, T.; Raison, P. E.; Somers, J.; Konings, R. J. M. Further insights into the chemistry of the Bi-U-O system. *Dalton Trans.* 2016, *45*, 7847-7855; (e) Vitova, T.; Green, J. C.; Denning, R. G.; Loble, M.; Kvashnina, K.; Kas, J. J.; Jorissen, K.; Rehr, J. J.; Malcherek, T.; Denecke, M. A., Polarization dependent high-energy resolution X-ray absorption study of dicesium uranyl tetrachloride. *Inorg. Chem.* 2015, *54*, 174-182; (f) Vitova, T.; Pidchenko, I.; Fellhauer, D.; Bagus, P. S.; Joly, Y.; Prüßmann, T.; Bahl, S.; González-Robles, E.; Rothe, J.; Altmaier, M.; Denecke, M. A.; Geckeis, H. The role of the 5f valence orbitals of early actinides in chemical bonding. *Nat. Comm.*, 2017, *8*, 16053.

[13] Bahl, S.; Peuget, S.; Pidchenko, I.; Prüßmann, T.; Rothe, J.; Dardenne, K.; Delrieu, J.; Fellhauer, D.; Jégou, C.; Geckeis, H.; Vitova T. Pu Coexists in Three Oxidation States in a Borosilicate Glass: Implications for Pu Solubility. *Inorg. Chem*. 2017, *56*, 13982-13990.

[14] Li, Y.; Burns, P. C. The crystal structure of synthetic grimselite. *Can. Mineral.* 2001, *39*. 1147-1151.

[15] Nipruk, O.; Knyazev, A.; Chernorukov, G.; Pykhova, Y. Synthesis and study of hydrated uranium(VI) oxides, UO3·nH2O. *Radiochem.* 2011, *53*, 146-150.

[16] Rothe, J.; Butorin, S.; Dardenne, K.; Denecke, M. A.; Kienzler, B.; Loble, M.; Metz, V.; Seibert, A.; Steppert, M.; Vitova, T.; Walther, C.; Geckeis, H. The INE-Beamline for actinide science at ANKA. *Rev. Sci. Instrum.* 2012, *83*, 043105.

[17] (a) Zimina, A.; Dardenne, K.; Denecke, M. A.; Doronkin, D. E.; Huttel, E.; Lichtenberg, H.; Mangold, S.; Prüßmann, T.; Rothe, J.; Spangenberg, T.; Steininger, R.; Vitova, T.; Geckeis, H.; Grunwaldt, J.-D. CAT-ACT-A new highly versatile x-ray spectroscopy beamline for catalysis and radionuclide science at the KIT synchrotron light facility ANKA. *Rev. Sci. Instrum.*, 2017, *88*, 113113; (b) Kleymenov, E. et al. Five-element Johann-type X-ray emission spectrometer with a single-photon-counting pixel detector. *Rev. Sci. Instrum.* 2011, *82*, 065107.

[18] (a) Walshe, A.; Prüßmann, T.; Vitova, T.; Baker, R. J. An EXAFS and HR-XANES study of the uranyl peroxides $[UO_2(\eta^2\text{-}O_2)(H_2O)_2]\cdot nH_2O$ (n = 0, 2) and uranyl (oxy)hydroxide $[(UO_2)_4O(OH)_6].6H_2O$. *Dalton Trans*. 2014, *43*. 4400-4407; (b) Glatzel, P.; Bergmann, U. High resolution 1s core hole X-ray spectroscopy in 3d transition metal complexes - electronic and structural information. *Coord. Chem. Rev.* 2005, *249*. 65-95.

[19] Solé, V.A.; Papillon, E.; Cotte, M.; Walter, Ph.; Susini, J. A multiplatform code for the analysis of energy-dispersive X-ray fluorescence spectra. *Spectrochim. Acta Part B* 2007, *62* 63-68.

[20] Ravel, B.; Newville, M. ATHENA, ARTEMIS, HEPHAESTUS: data analysis for X-ray absorption spectroscopy using IFEFFIT. *J Synchrotron Radiat* 2005, *12*, 537-541.

[21] Volkov, Y. F.; Visyashcheva, G. I.; Tomilin, S. V.; Kapshukov, I. I.; Rykov, A. G. Determination of the crystal structure of $M_3AnO_2(CO_3)_2.nH_2O$. *Radiokhimiya* 1981, *23*, 243-247.

[22] Rehr, J. J.; Kas, J. J.; Vila, F. D.; Prange, M. P.; Jorissen, K. Parameter-free calculations of X-ray spectra with FEFF9. *Phys. Chem. Chem. Phys.* 2010, *12*, 5503-5513.

[23] (a) Vitova, T.; Kvashnina, K. O.; Nocton, G.; Sukharina, G.; Denecke, M. A.; Butorin, S. M.; Mazzanti, M.; Caciuffo, R.; Soldatov, A.; Behrends, T.; Geckeis, H. High-energy resolution x-ray absorption spectroscopy study of uranium in varying valence states. *Phys. Rev. B* 2010, *82* 235118; (b) Bunau, O.; Joly, Y. Self-consistent aspects of X-ray absorption calculations. *J. Phys. Condens. Matter*, 2009, *21*, 345501.

[24] Keenan, T. K.; Kruss, F. H. Potassium Double Carbonates of Pentavalent Neptunium, Plutonium, and Americium. *Inorg. Chem.*1964, *39*, 1231-1232.

[25] Parkhurst, D. L. Appelo, C. A. J. Description of input and examples for PHREEQC version 3—a computer program for speciation, batch-reaction, one-dimensional transport, and inverse geochemical calculations. US geological survey techniques and methods, 2013, *6*, 497.

[26] M. Grivé, L. Duro, E. Colàs, E. Giffaut, Thermodynamic data selection applied to radionuclides and chemotoxic elements: An overview of the ThermoChimie-TDB. *Appl. Geochem.* 2015, *55*, 85-94.

[27] Update on the chemical thermodynamics of uranium, neptunium, plutonium, americium and technetium. ed. Guillaumont, R.; Mompean F. J. Elsevier 2003 Amsterdam.

[28] Kaszuba, J. P.; Runde, W. H., The aqueous geochemistry of neptunium: Dynamic control of soluble concentrations with applications to nuclear waste disposal. *Environmental Science and Technology* **1999,** *33*, 4427-4433.

[29] Novak, C. F.; Mahamid, I. A.; Becraft, K. A.; Carpenter, S. A.; Hakem, N.; Prussin, T. Measurement and thermodynamic modeling of Np(V) solubility in aqueous K_2CO_3 solutions to high concentrations. *J. Solution Chem.* 1997, *26*, 681-697.

[30] Fanghänel, Th.; Neck, V.; Kim, J. I. Thermodynamics of neptunium(V) in concentrated salt solutions: II. Ion interaction (Pitzer) parameters for Np(V) hydrolysis species and carbonate complexes. *Radiochim Acta*, 1995, *3*, 169.

[31] Neck, V.; Runde, W.; Kim. J.I. Solid-liquid equilibria of neptunium(V) in carbonate solutions of different ionic strengths II. Stability of the solid phases. *J. Alloys Compd*. 1995, *225* 295-302.

[32] (a) Keenan, T. K.; Kruse, F. H. Potassium double carbonates of pentavalent neptunium, plutonium, and Americium. *Inorg. Chem.* 1964, *3*, 1231-1232; (b) Visyashcheva, G. I.; Volkov, Y. F.; Simakin, G. A.; Kapshukov, I. I.; Bevz, A. S.; Yakovlev, G. N. Composition and some properties of solid carbonates of pentavalent neptunium with potassium obtained from K_2CO_3 solutions. *Radiokhimiya* 1974, *16*, 853-859.

[33] (a) Volkov, Y. F.; Kapshukov, I. I.; Visyashcheva, G. I.; Yakovlev, G. N. X-ray investigation of neptunium (V), plutonium (V), and americium (V) monocarbonates with potassium. *Radiokhimiya* 1974, *16*, 863-867; (b) Volkov, Y. F.; Tomilin, S. V.; Visyashcheva, G. I.; Kapshukov, I. I. X-ray structure analysis of $LiNpO_2CO_3$ and $NaNpO_2CO_3$. *Radiokhimiya* 1979, *21*, 668-672; (c) Volkov, Y. F.; Visyashcheva, G. I.; Kapshukov, I. I. Production and identification of hydrate forms of sodium monocarbonatoneptunaylate. *Radiokhimiya* 1977, *19*. 319-323; (d) Volkov, Y. F.; Visyashcheva, G. I.; Kapshukov, I. I.; Simakin, G. A.; Yakovlev, G. N. Composition and properties of carbonates of the pentavalent actinides. *Radiokhimiya* 1976, *18*, 96-100.

[34] Finch, R. J.; Cooper, M. A.; Hawthorne, F. C.; Ewing. R. C. Refinement of the crystal structure of rutherfordine, *Can. Mineral*. 1999, *37*, 929-938.

[35] Biswas, S.; Steudtner, R.; Schmidt, M.; McKenna, C.; Leon Vintro, L.; Twamley, B.; Baker, R. J., An investigation of the interactions of Eu^{3+} and Am^{3+} with uranyl minerals: implications for the storage of spent nuclear fuel. *Dalton Trans.* 2016, *45*, 6383-6393.

[36] Vochten, R.; Deliens, M. Blatonite, $UO_2CO_3 \cdot H_2O$, a new uranyl carbonate monohydrate from San Juan County, Utah. *Can. Mineral.* 1998, *36*. 1077-1081.

[37] (a) Fellhauer, D.; Neck, V.; Altmaier, M.; Lützenkirchen, J.; Fanghänel, T. Solubility of tetravalent actinides in alkaline $CaCl_2$ solutions and formation of Ca-4[An(OH)(8)](4+) complexes: A study of Np(IV) and Pu(IV) under reducing conditions and the systematic trend in the An(IV) series. *Radiochim. Acta* 2010, *98*. 541-548; (b) Fellhauer, D.; Rothe, J.; Altmaier, M.; Neck, V.; Runke, J.; Wiss, T.; Fanghänel, T. Np (V) solubility, speciation and solid phase formation in alkaline CaCl2 solutions. Part I: Experimental results. *Radiochim. Acta* 2016, *104*, 355-379; (c) Gaona, X.; Fellhauer, D.; Altmaier, M. Thermodynamic description of Np (VI) solubility, hydrolysis, and redox behavior in dilute to concentrated alkaline NaCl solutions. *Pure Appl. Chem.* 2013, *85*, 2027-2049.

[38] Gaona, X., Fellhauer, D., Rothe, J. Altmaier, M. Investigations on Np(VI) in alkaline NaCl solutions: aqueous chemistry and solid phase characterization (pgs. 343-352), in “4th Annual Workshop Proceedings of the Collaborative Project "Redox Phenomena Controlling Systems" (7th EC FP CP RECOSY)”, Marcus, M., Kienzler, B., Duro, L., Grivé, M. Montoya, V. (eds.), KIT Scientific Publishing, Karlsruhe, 2012. (ISBN: 978-3-86644-921-3)

39 Gaona, X.; Tits, J.; Dardenne, K.; Liu, X.; Rothe, J.; Denecke, M. A.; Wieland, E.; Altmaier, M., Spectroscopic investigations of Np(V/VI) redox speciation in hyperalkaline TMA-(OH, Cl) solution. *Radiochim. Acta* 2012, *100*, 759-770.

[40] Podkovyrina, Y.; Pidchenko, I.; Prüßmann, T.; Bahl, S.; Soldatov, A.,;Vitova, T., presented in part at 16th International Conference on X-ray Absorption Fine Structure, Karlsruhe, Germany, 23-28 August 2015.

[41] Vitova, T.; Pidchenko, I.; Biswas, S.; Beridze, G.; Dunne, P. W.; Schild, D.; Wang, Z.; Kowalski, P. M.; Baker, R. J. Dehydration of the Uranyl Peroxide Studtite, [UO2(η2-O2)(H2O)2]·2H2O, Affords a Drastic Change in the Electronic Structure: A Combined X-ray Spectroscopic and Theoretical Analysis. *Inorg. Chem.* 2018, 57, 1735-1743.

[42] (a) Zegke, M.; Zhang, X.; Pidchenko, I.; Hlina, J. A.; Lord, R. M.; Purkis, J.; Nichol, G. S.; Magnani, N.; Schreckenbach, G.; Vitova, T.; Love, J. B.; Arnold, P. L. *Chem. Sci.* 2019, *10*, 9740-9751; (b) Hunault, M.O.J.Y.; Lelong, Cormier, G.; L.; Galoisy, L.; Solari, P. –L.; Calas G. Speciation Change of Uranyl in Lithium Borate Glasses. *Inorg. Chem*. 2019, *58*, 6858−6865.

[43] Hayton, T. W. Understanding the origins of O_{yl}–U–O_{yl} bending in the uranyl (UO_2^{2+}) ion.

Dalton Trans., 2018, *47*, 1003-1009

[44] Grigor'ev, M. S.; Krot, N. N. Synthesis and single crystal X-ray diffraction study of U(VI), Np(VI), and Pu(VI) perchlorate hydrates. *Radiochemistry* 2010, *52*. 375-381.

[45] Fellhauer, D. Untersuchungen zur Redoxchemie und Löslichkeit von Neptunium und Plutonium. PhD thesis, University of Heidelberg, Germany (2013).

[46] Vitova, T.; Pidchenko, I.; Fellhauer, D.; Pruessmann, T.; Bahl, S.; Dardenne, K.; Yokosawa, T.; Schimmelpfennig, B.; Altmaier, M.; Denecke, M.; Rothe, J.; Geckeis, H. Exploring the electronic structure and speciation of aqueous and colloidal Pu with high energy resolution XANES and computations. *Chem. Commun*. 2018, *54*, 12824-12827.

[47] Burns, P. C. and Klingensmith, A. L. Uranium mineralogy and neptunium mobility. *Elements*, 2006, *2*, 351-356.

[48] Meredith, N. A.; Polinski, M. J.; Cross, J. N.; Villa, E. M.; Simonetti, A.; Albrecht-Schmitt, T. E. Synthetic Influences on Neptunium Incorporation in Naturally Occurring Copper Uranyl Phosphates. *Cryst. Growth Des* 2013, *13*, 386-392.

[49] Hay, P. J., Martin, R. L. & Schreckenbach, G. Theoretical studies of the properties and solution chemistry of AnO_2^{2+} and AnO_2^{+} aquo complexes for An = U, Np, and Pu. *J. Phys. Chem. A* 2000, *104*, 6259–6270; (b) Clark, D. L., Hecker, S. S., Jarvinen, G. D. & Neu, M. P. in The Chemistry of the Actinide and Transactinide Elements (eds Morss, L. R., et al.) 813–1264 (Springer, 2006).

For TOC only

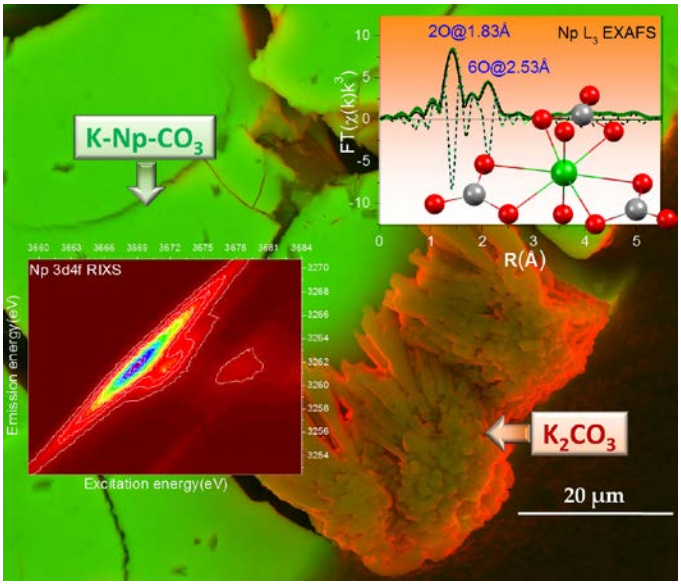

Synopsis:

Our observation that neptunyl(V) carbonates precipitate in preference to uranyl(VI) carbonates in a alkaline K-Na-CO_3-H_2O system is important for understanding the fundamental chemical behavior of actinides. It is demonstrated that $K[NpO_2CO_3]_{(cr)}$, $K_3[NpO_2(CO_3)_2]\cdot nH_2O_{(cr)}$ and $K_3Na[UO_2(CO_3)_3]\cdot H_2O_{(cr)}$ are the main solid phases formed. Np 3d4f RIXS and M_5 edge HR-XANES are applied for oxidation state and coordination studies of Np for the first time. We reveal that the Np M_5 edge HR-XANES is sensitive to the Np-Oaxial bond length in neptunyl(V)/(VI).